Faculty of Engineering and Technology

Department of Electrical, Computer and Telecommunications

DESIGN AND IMPLEMENTATION OF A RECONFIGURABLE METASURFACE ANTENNA

by

BOKAMOSO KEBATHO LEDIMO

Student ID number: 14000384

MEng Computer and Telecommunications

A Thesis Submitted to the Faculty of Engineering and Technology in Partial Fulfilment of the Requirements for the Award of the Degree of Master of Engineering in Computer and Telecommunications of BIUST

Supervisor: Dr. Bokamoso Basutli

Department of Electrical, Computer and Telecommunications

Faculty of Engineering and Technology, BIUST

basutlib@biust.ac.bw

Co-supervisor: Dr. Modisa Mosalaosi

Department of Electrical, Computer and Telecommunications

Faculty of Engineering and Technology, BIUST

mosalaosim@biust.ac.bw

January, 2022

Contents

List of Figures iv

List of Tables vi

Mathematical Notations vii

Abstract viii

Acknowledgements x

List of Abbreviations xi

1 A Review of Reconfigurable Metasurfaces 1

1.1 Introduction 1

1.2 Background 3

1.2.1 Metamaterials: Concept 4

DNG Metamaterial 6

1.2.2 Evolution of Metamaterials 7

1.3 Problem Statement 9

1.4 Research Objectives 9

1.4.1 Contributions 10

1.5 Thesis Outline 10

1.6 Conclusion 11

2 Electromagnetic Manipulation: An Evolution 12

2.1 Introduction 12

2.2 RMS design considerations 13
2.3 Implementation of RMS 15
2.3.1 Optical Tunable Metasurfaces (OTMs) 15
Voltage-controlled tuning of a lumped element 17
Thermal tuning 21
Magnetic Tuning 25
2.4 Applications of reconfigurable metasurfaces 27
2.5 Conclusion 29

3 Design Procedure of Metasurface Unit Cell 31
3.1 Introduction and Related Works 31
3.2 Theoretical formulation 33
3.3 Conclusion 38

4 Design Procedure of a Frequency Reconfigurable Metasurface Antenna at mmWave Band 40
4.1 Introduction 40
4.1.1 Related Works 42
4.1.2 Contribution 43
4.2 Proposed Methodology 43
4.3 Simulation Processes 46
4.4 Results and Analysis 48
4.4.1 Reflection Coefficient 49
4.4.2 Reflection Phase 51
4.4.3 Gain and Directivity 52
4.4.4 Effective Permittivity and Permeability 55
4.4.5 Comparison with Previous Work 56
4.5 Conclusion 57

5 Conclusion **59**

5.1 Future Work 60

References **61**

List of Figures

1.1 From meta-atoms to metamaterials 4

1.2 Metamaterial classifications based on permittivity and permeability values. 5

1.3 Creating DNG metamaterials by combining wires and SRR 6

1.4 Snell's law of reflection 8

2.1 Top and side view of metasurface structure 13

2.2 Parameters to consider when designing RMSs [1] 14

2.3 System concept that combines software-defined metasurfaces with an embedded network of controllers that allows actuation, sensing and processing of information by [2]. 21

2.4 Ge–Sb–Te phase diagram illustrating important pseudo-binaries . . . 23

2.5 Schematic diagram of magnetic tunable metasurface 25

2.6 Two main applications of reconfigurable metasurface. 28

3.1 Geometry of SRR 32

3.2 Equivalent circuit with gap capacitances taken into account 34

4.1 Proposed metasurface unit cell 44

4.2 A 4×4 RMS integrated with PIN diodes 48

4.3 Return loss results of metasurface unit cell before and after optimization 49

4.4 Return loss simulation results of 16 element metasurface array with and without PIN diodes. 50

4.5 Reflection phase of 16 element metasurface array with and without PIN diodes. 52
4.6 Directivity and Gain of 16 element metasurface array with and without PIN diodes. 53
4.7 Retrieved effective constitutive parameters of the simulated results . 56

List of Tables

1.1 Different terms used in metasurface technologies [3]. 3

4.1 Summary of calculation of dimensions of a metasurface unit cell . . . 47

4.2 Unit cell dimensions before and after software optimization 47

4.3 Summary of return loss and bandwidth results 50

4.4 Summary of gain, directivity and radiation efficiency 54

4.5 Comparisons between proposed 16 elements frequency RMS and existing designs 57

BOTSWANA INTERNATIONAL UNIVERSITY OF SCIENCE & TECHNOLOGY

POSTGRADUATE SCHOOL

Declaration Regarding the Work and Copyright

DECLARATION REGARDING THE WORK AND COPYRIGHT

Candidate (please write in caps or type): BOKAMOSO KEBATHO LEDIMO

Student ID: 14000384

Thesis Titled: Design and Implementation of a Reconfigurable Metasurface Antenna

I, **Bokamoso Kebatho Ledimo**, certify that the Thesis is all my own original work and that I have not obtained a degree in this University or elsewhere on the basis of any of this work.

(If the thesis is based on a group project, then the student must indicate the extent of her / his contribution, with reference to any other theses submitted or published by each collaborator in the project, and a declaration to this effect must be included in the thesis)

This thesis is copyright material protected under the Berne Convention, the Copyright and Neighbouring Rights Act, Act. No. 8 of 2000 and other international and national enactments, in that behalf, on intellectual property. It must not be reproduced by any means, in full or in part, except for short extracts in fair dealing; for researcher private study, critical scholarly review or discourse with an acknowledgement, without the written permission of the office of the Postgraduate School, on behalf of both the author and the BIUST.

Signed: ---------- Date: 30/05/2022

Primary Supervisor (please write in caps or type): DR BOKAMOSO BASUTLI

I, Dr. Bokamoso Basutli, hereby confirm that I have inspected the above titled thesis and, to the best of my knowledge, it is based on the original work of the candidate.

Signed: ---------- Date: 30 May 2022

Abstract

The use of the millimeter wave (mmWave) spectrum and further exploration of sub-mmWave has led to a new era in wireless communication, as the need for higher data rates grows. High frequencies, on one hand, incur a higher path loss, requiring an increase in antenna gain requirements. Metasurfaces, which emerge as a promising technology for mitigating path loss effects by utilizing 2D arrays of engineered meta-atoms resembling metamaterials that control the surface's electromagnetic response has been introduced. Currently, they are primarily considered as passive reflecting devices in wireless communications, assisting conventional transceivers in shaping propagation environments. The work herein presents an alternative application of metasurfaces for wireless communications as active reconfigurable antennas for next generation transceivers. A framework that demonstrates the design process of a metasurface antenna structure is introduced and further used to design a 4×4 array and its reconfigurable counterpart. In contrast to conventional array antennas, a reconfigurable metasurface (RMS) antenna does not require phase-shifters and amplifiers, hence, leading to a reduction of costs. Instead, each individual element achieves reconfigurability by shifting the resonating frequency using semiconductor devices such as PIN diodes. The proposed metasurface antenna is designed to operate at a frequency of 28 GHz and 40 GHz. The work achieved a return loss of -18.57 dB and -22.0 dB, which indicates good impedance match between transmission line and antenna. In addition, an increase in gain and directivity is observed when diodes are added to the metasurface antenna array. However, as a result of diode losses, the radiation efficiency of the metasurface array decreased. Future directions have been explored that may pave way to present the full potential of active metasurface antennas in upcoming wireless communications.

This thesis is dedicated to Keloitsang and Keogalale Ledimo who taught me to always be patient with myself.

Acknowledgements

I humble myself before the Almighty God who protects me and gives me challenges which shape my life. I thank Him for all His blessings and guidance throughout. I would like to express my deep and sincere gratitude to my research supervisors, Dr. Bokamoso Basutli and Dr Modise Mosalaosi, for giving me the opportunity to carry out my research and providing invaluable guidance throughout. I'd like to thank my colleagues from the Signal Processing and Network Systems (SPNS) research group for helping me overcome some of the challenges I encountered during my studies. I would like to express my gratitude to the Department of Electrical, Computer and Telecommunications at the Botswana International University of Science and Technology for providing me with the computer facilities and the financial support I needed to complete my thesis.

I am extremely grateful to my parents Keloitsang Ledimo, Keogalale Ledimo, Grace Ledimo and my late father Gaselobelo Ledimo for their love, prayers, care and sacrifices for educating and preparing me for my future. Also, I express my thanks to Sithini Ndebele and my siblings (Helmet Ledimo, Tebogo and Tom Mcintyre, Titus and Masego Ledimo, Keaitse S. and Dr. Bonolo S. Ledimo) for their support and valuable prayers. Thank you for always being there for me. Your support has meant more to me than you could possibly realize.

Finally, I would also like to thank Bokamoso C. Otukile for his love and emotional support throughout my studies and all my close friends (Dr. Bunmi Olatoyinbo, Bonolo Molefe, Thabang Ntanda, Tsholofelo Mothupi and Gaamangwe Mosielele) for their continued support throughout.

List of Abbreviations

2D	Two-Dimensional
3D	Three-Dimensional
4G	Fourth-Generation
5G	Fifth-Generation
6G	Sixth-Generation
mmWave	Millimeter Wave
ADAS	Advanced Driver Assistance Systems
AI	Artificial Intelligence
AO-MM	Alternating Optimization-Minorization Maximization
BCD	Block Coordinate Descent
BER	Bit Error Rate
BS	Base Station
CNP	Charge Neutral Point
CR	Channel Randomization
CST MWS	Computer Simulation Technology Microwave Studio
DNG	Double Negative
DPS	Double Positive
DTD	Data Transmission Duration
EE	Energy Efficiency
EH	Energy Harvesting
EHR	Energy Harvesting Receiver
EM	Electromagnetic
ENG	Epsilon Negative
FDTD	Finite Difference Time Domain
FMR	Ferro Magnetic Resonance
FPGA	Field Programmable Gate Array
GaAs	Gallium Arsenide
HAP	High Altitude Platform
ID	Information Decoding
IFFT	Inverse Fast Fourier Transform
IRS	Intelligent Reflective Surface
LIS	Large Intelligent Surface
LOS	Line-of-Sight
MEMS	Micro Electro-Mechanical Systems
MIMO	Multiple-Input Multiple-Output
MISO	Multiple-Input Single-Output
MNG	Mu Negative
NOMA	Non-Orthogonal Multiple Access
OMA	Orthogonal Multiple Acces

OTM	Optical Tunable Metasurface
PCM	Phase Change Materials
PIS	Passive Intelligent Surface
PLS	Physical Layer Security
PSD	Pilot Signal Duration
QoS	Quality of Service
RE	Rate Energy
RF	Radio Frequency
RFSS	Reconfigurable Frequency Selective Surface
RIS	Reconfigurable Intelligent Surface
RMS	Reconfigurable Metasurface
SDM	Software-Defined Metasurface
SDMA	Spatial Division Multiple Access
SDR	Semi-Definite Relaxation
SDS	Software-Defined Surface
SINR	Signal to Interference Noise Ratio
SRA	Smart Reflect-Array
SRR	Split Ring Resonator
SWIPT	Simultaneous Wireless Information and Power Transfer
TDD	Time Division Duplex
THz	Tetra Hertz
UAV	Unmanned Aerial Vehicles
UE	User Equipment
UNDSG	United Nations Sustainable Development Goals
V2I	Vehicles-to-Infrastructures
V2V	Vehicles-to-Vehicles
V2X	Vehicles-to-Everything
VANET	Vehicular Adhoc Network
VRU	Vulnerable Road Users
WSR	Weighted Sum Rate

Chapter 1

A Review of Reconfigurable Metasurfaces

1.1 Introduction

The rapid growth of smart terminals and emerging new applications (e.g. real-time and interactive services), has drastically increased wireless data traffic. This has affected existing cellular networks, including the ongoing fifth-generation (5G), as it cannot completely match the increasing technological demand [4]. In an attempt to address the challenges brought about by increased traffic demands, 5G utilizes technologies such as multiple-input multiple-output (MIMO) and mmWaves [5]. As a result, 5G has demonstrated its potential for ultra-high speed, high capacity, ultra-low latency, and high reliability [6,7]. However, there are other crucial issues that have not been resolved such as high propagation losses which limit the range of communication [8].

As indicated in [9], it is impossible for all the requirements of the 5G applications to be supported by a single enabling technology hence why these crucial issues are still pending. In accordance with the launch of 5G, further research is being conducted by industries, academia, and government in order to develop the 6G mobile communication system to attain higher system capacity, data rates and improved quality

of service (QoS) [5, 10–14]. 6G is structured to incorporate 3 major aspects, i.e, mobile ultra-broadband, super internet of things (IoT) and artificial intelligence (AI), where typical use cases are anticipated for each aspect [10]. For this reason, new use cases, user requirements and networking trends for 2030 and beyond may bring more challenging communication engineering problems, which necessitate radically new communication paradigms in the physical layer [10]. Nevertheless, under the United Nations sustainable development goals (UN SDG), it is intended for 6G to introduce a new phase of "Internet of Intelligence" through which people will be intelligently linked with things [15]. Some of the 17 UN SDGs aim to apply 6G technologies on issues such as climate change, inequality and poverty with the aim to sustain world economies.

All the generations preceding to 5G and 6G have been focused on the improvement and optimization of hardware and software of the transmitter and receiver side. In order to improve the QoS wireless communications, there has been a rising urgency in controlling the unpredictable random characteristics of the wireless propagation environment [16]. This can be done via metasurface technology which is commonly used to design and control the two-dimensional (2D) distribution of the scattering characteristics [5, 17–19]. Among technologies envisaged for 6G, metasurfaces appear to be a promising technology for forthcoming wireless communication network systems especially in reconfiguring the wireless propagation environment [20–24]. The literature uses several terms interchangeably to describe metasurface technologies, such as intelligent reflective surface (IRS), reconfigurable intelligent surface (RIS), large intelligent surface (LIS) and reconfigurable metasurface (RMS). Despite their similarities, each of these terminologies emphasizes a different aspect of the smart surface [11]. Authors in [3] presented a comparison of such various terms in Table 1.1.

TABLE 1.1: Different terms used in metasurface technologies [3].

Surface Term	**Explanation**
Intelligent reflecting surfaces (IRS)	Focuses on the reflective properties of the smart surface.
Large intelligent surfaces (LIS)	Considers a large surface length or an immense number of antennas.
Passive intelligent surfaces (PIS)	Underlines the powerless passive reflection properties
Reconfigurable intelligent surfaces (RIS)	Highlights the ability to reconfigure the smart surface for incident signals.
Reconfigurable metasurfaces (RMS)	The metallic pattern through which the surface is engineered is highlighted. The focus is on how the structure is designed.
Software-defined surfaces (SDS)	Analyzes the software-defined interaction between incoming waves and the surface.
Software-defines metasurfaces (SDM)	Both the metallic pattern and the software-defined function are highlighted.
Large intelligent metasurfaces (LIM)	Analyzes metasurfaces asymptotically using a massive number of antennas.
Smart reflect-arrays (SRA)	Emphasizes on the reflection function.

This thesis proposes the design of a frequency reconfigurable metasurface operating in the mmWave frequency band therefore the term "Reconfigurable Metasurfaces" will be used.

1.2 Background

The concept of "reflection" was mimicked from our everyday mirror objects which reflect an image thus making them an example of reflecting surfaces. A brief overview

of what makes up the RMS technology is provided in this section.

1.2.1 Metamaterials: Concept

In recent years, scientists have embarked on research regarding the use of artificial materials which generate significant benefits and introduces various applications. Metamaterials are among these artificial materials as they are composed of closely spaced sub-wavelength meta-atoms which resonantly couple to both the electric or magnetic components of the incident electromagnetic fields, thereby exhibiting properties that are not found in nature as shown in Figure 1.1 [25–27].

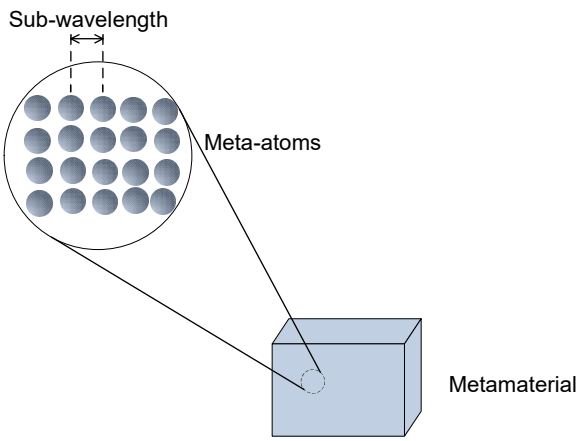

FIGURE 1.1: From meta-atoms to metamaterials

Consequently, they have physical properties that are largely determined by their structures rather than their individual attributes. Furthermore, different structures influence the categorization of metamaterials according to their electrical permittivity and magnetic permeability denoted as ϵ and μ values respectively [28]. Authors in [29] made it possible to classify these materials in four different classes as shown in Figure 1.2.

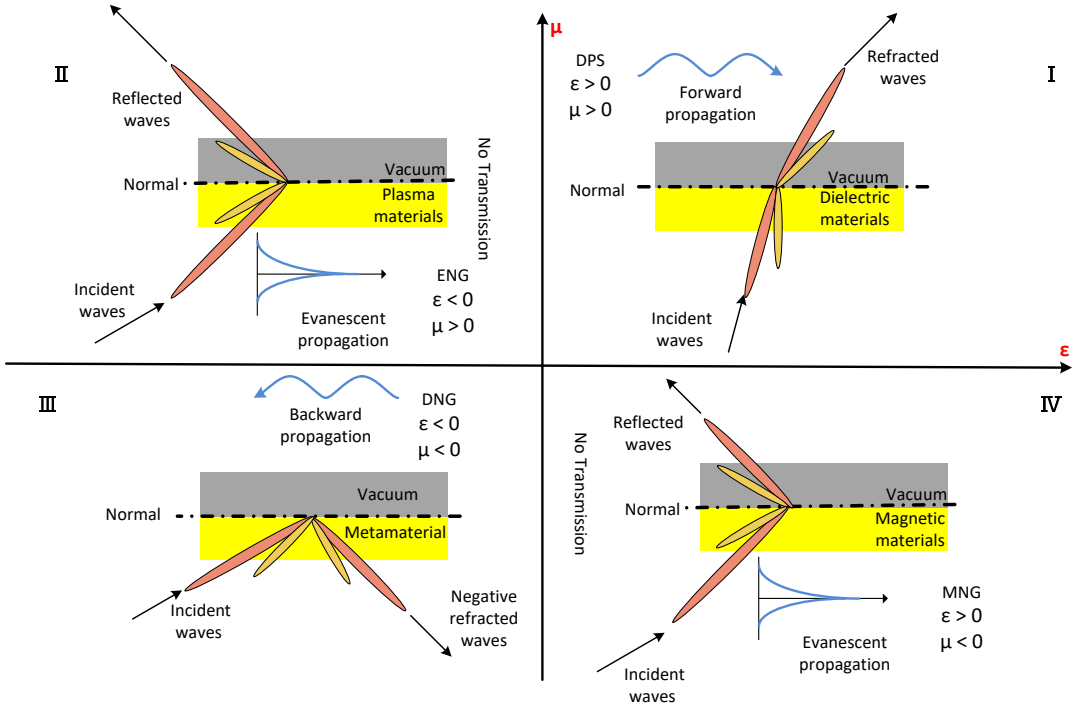

FIGURE 1.2: Metamaterial classifications based on permittivity and permeability values.

The first quadrant from Figure 1.2 is characterized by the existence of both positive ϵ and μ values. Such materials are known as double positive (DPS). These can be found in nature, for example, in dielectric materials where EM waves propagate. The second quadrant consists of materials that are represented by a plasma and are known as epsilon negative medium (ENG) due to ϵ<0 and μ>0 values [30]. The third quadrant is of interest being that both ϵ and μ values of materials are negative and not found in nature, hence why it is called the double negative medium (DNG). Furthermore when plane waves propagate in metamaterials, the electric field, magnetic field and wave vector adopt the left-hand rule hence why they are referred to as left-handed materials [31]. The fourth quadrant is called the mu negative medium (MNG) represented by magnetic materials as it entails positive ϵ and negative μ values. From Figure 1.2, it is observed that the majority of waves propagate through two mediums namely; region I and III.

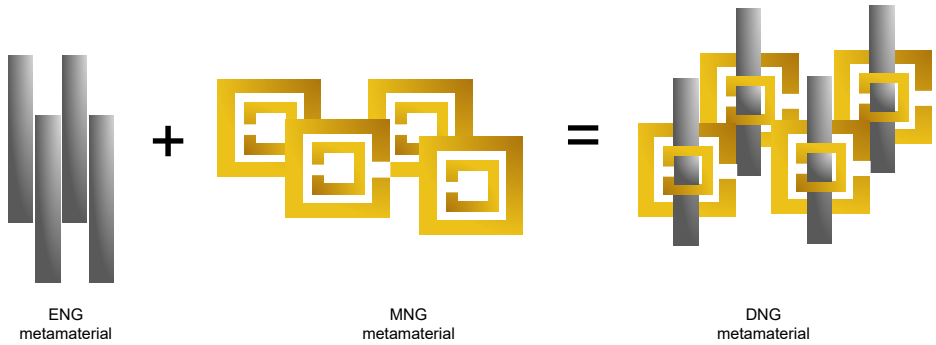

FIGURE 1.3: Creating DNG metamaterials by combining wires and SRR

Presently, most metamaterials are being designed with two basic types of structures: dense arrays of thin wires (the electric dipoles) and arrays of split-ring resonators (SRRs) (the magnetic loops) [32]. In order to attain DNG mediums, ENG and MNG mediums are combined as shown in Figure 1.3. This thesis will focus on the third quadrant as they give metamaterials the phenomenon to control EM waves.

DNG Metamaterial

The combination of MNG and ENG mediums not only meets the requirement of ϵ<0 from a wire medium and μ<0 from an SRR, their strong resonance properties are able to influence the frequency (Drude-Lorentz models) [33]. As a result, the generated DNG metamaterials depend on frequency, so that the refractive index n is reformatted as follows:

$$n \equiv n_{\text{eff}}(\omega) = \sqrt{\epsilon_{\text{eff}}(\omega)\mu_{\text{eff}}(\omega)}, \tag{1.1}$$

where $\epsilon_{\text{eff}}(\omega)$ and $\mu_{\text{eff}}(\omega)$ are the frequency-dependent effective permittivity and permeability respectively [30]. According to [30,34], Drude-Lorentz dispersion models characterizes these material parameters, which have the form shown in equation (1.2) and (1.3)

$$\epsilon_{\text{eff}}(\omega) = 1 - \frac{\omega_{ep}^2 - \omega_{e0}^2}{\omega^2 - \omega_{e0}^2 + j\omega\delta_e}, \tag{1.2}$$

$$\mu_{\text{eff}}(\omega) = 1 - \frac{\omega_{mp}^2 - \omega_{m0}^2}{\omega^2 - \omega_{m0}^2 + j\omega\delta_m}, \tag{1.3}$$

where

- ω is the frequency of the propagating EM wave
- ω_{ep} and ω_{mp} are the electric and magnetic plasma frequencies respectively
- ω_{e0} and ω_{m0} are the electric and magnetic resonant frequencies respectively
- δ_e and δ_m are the electric and magnetic damping frequencies respectively

1.2.2 Evolution of Metamaterials

As a 2D counterpart to metamaterials, metasurfaces are a semi-periodic arrangement of apertures or scatterers that allow for certain engineering properties [35,36]. As a periodic (or aperiodic) structure, metasurfaces have individual elements (scatterers) with thickness and periodicity much less than the wavelength of operation. Alternatively, metasurfaces can be defined as a symmetric or asymmetric array of resonant scatterers that control the surface's electromagnetic response [37]. Furthermore, according to [38], the term metasurface refers to an electromagnetic discontinuity, which in practice is an electromagnetic structure that is sub-wavelength in thickness, electrically large in transverse size, and consists of scattered particles with ultra-small features. In [39], authors described metasurfaces as simply 2D arrays of sub-wavelength metallic or dielectric particles that change electromagnetic waves in different ways. They further mentioned that the physical arrangement of the scattering particles (e.g., full or slotted patches, straight or curved strips, various types of crosses) determines how the metasurface transforms an incident wave into a specified reflected or transmitted signal [40].

A metasurface does not necessarily have the same angles of incidence and reflection as a conventional surface. When an incident wave d_i arrives on a reflective surface at an angle θ_i, it bounces off on the surface at the same angle but in opposite direction

[41, 42]. It is then called the reflected (scattered) wave d_r at an angle of θ_r. This phenomenon is called Snell's law of reflection as depicted in Figure 1.4,

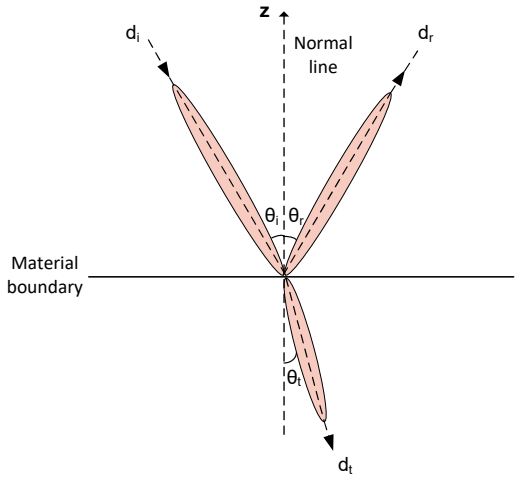

FIGURE 1.4: Snell's law of reflection

where θ_i and θ_r represent the angle of incident and reflection, respectively. The angles of reflection and refraction are only dependent upon the material properties at either side of the boundary as well as the angle of incident EM waves. However, EM waves cannot be steered in any other direction between the two materials due to the boundary between them. In contrast, when an appropriately designed metasurface is placed between the two materials, the EM wave's behavior can be more easily controlled.

By modifying their permittivity and permeability values, metamaterials can control the propagation of light, but they still rely on the propagation effect to manipulate electromagnetic waves [37]. On one hand, metamaterials manipulate a wave over an extremely thin layer, which results in relatively bulky structures [43]. On the other hand, metasurfaces are less bulky and provide lower loss structures due to their 2D nature [35]. Metamaterials are also complex to fabricate because of their 3D nature, however, metasurfaces are a promising alternative as the planar structure allows for their easy fabrication [26]. In addition, the planar fabrication process is highly cost-effective when compared to the creation of complex 3D metamaterials. Recently, the

scientific community has shown a keen interest in metasurfaces due to their various advantages over metamaterials. Therefore, metasurfaces have allowed for applications such as controllable "smart" surfaces, miniaturized cavity resonators, novel wave-guiding structures, compact and wide-angle absorbers, impedance-matching surfaces.

1.3 Problem Statement

Due to the demand for uninterrupted connectivity and quality of service to users and devices, connected objects in harsh propagation environments has increased usage of the mmWave bands. Furthermore, the use of high frequencies for high data rates also increases path losses, which leads to increased antenna gain requirements. Therefore, there is a need for wireless communication antenna hardware that enables wireless communications to adapt to changes in radio environment in order to maximize system performance.

1.4 Research Objectives

Given the current literature review, it is evident that there is lack of a well documented process in the design of reconfigurable metasurface antenna which is one of the key processes needed in the current research where metamaterials have been identified as enablers for better antenna gain. The objective of this thesis is to design and implement a reconfigurable metasurface antenna by

- Proposing a framework demonstrating the design process of a metasurface antenna structure.
- Evaluating the proposed framework by proposing a frequency reconfigurable metasurface antenna for mmWave applications at 28 GHz and 40 GHz.

- Comparing and evaluating the performance of the proposed reconfigurable metasurface antenna against non reconfigurable.

1.4.1 Contributions

The contribution of this thesis is mainly on the design and simulation of a 4×4 frequency reconfigurable metasurface antenna using the proposed methodology for mmWave band applications. This contribution is supported by the following publication.

- **B. K. Ledimo**, P. Moaro, R. Ramogomana, M. Mosalaosi and B. Basutli, "Design Procedure of a Frequency Reconfigurable Metasurface Antenna at mmWave Band." Telecom 2022, 3, 379-395. https://doi.org/10.3390/telecom3020020.

1.5 Thesis Outline

This thesis explores reconfigurable metasurface antennas with potential applications in the next generation of mobile communications. The rest of the thesis is organized as follows.

This chapter presents an introduction of the thesis and its objectives.

Chapter 2 presents a review of existing implementation methods of RMS structures and the technology applications. The purpose of this chapter is to introduce the basic concepts and working principles of tunable, programmable, and intelligent metasurfaces. Additionally, design considerations of RMS structures are discussed.

Chapter 3 describes the existing theoretical analysis of designing square and circular split ring resonators which are the building blocks of metasurface structures.

Chapter 4 introduces a design concept of square split resonators which was used to implement a 4×4 metasurface antenna array. Furthermore, diodes were added to the array structure in order to achieve frequency reconfigurability. Parameters such

as the reflection coefficient, bandwidth, reflection phase, gain, and directivity of the proposed design was analyzed.

Chapter 5 presents the conclusions of this thesis, projected future work, and possible uses of the developed reconfigurable metasurface antenna.

1.6 Conclusion

Metasurfaces are 2D metamaterials that have electromagnetic properties that are not found in nature. Over the past two decades, much research has been conducted on metamaterials and metasurfaces, which are capable of exhibiting fascinating electromagnetic properties that cannot be achieved with naturally occurring materials. Due to demand for uninterrupted connectivity, these properties can be used to improve wireless communication networks by controlling the wireless propagation environment.

Chapter 2

Electromagnetic Manipulation: An Evolution

The goal of this chapter is to highlight the development of tunable, programmable, and intelligent metasurfaces, focusing on their basic concepts and working principles. The research opportunities associated with the integration of RMS and other emerging technologies is discussed. RMSs are electromagnetically thin sheets with tunable EM capabilities [44]. An important feature of this technology is to have a material whose EM properties can be altered by external stimuli.

2.1 Introduction

Over the course of developing metasurfaces, the limitations of fixed response metasurfaces in realistic applications, that is, limited working bandwidths and fixed wave manipulation capabilities were realized [45]. As a result, many efforts have been devoted to developing tunable/reconfigurable metasurfaces that can actively control EM waves with external tunings. Figure 2.1 shows a structure commonly used to implement a reconfigurable or tunable metasurface. The structure is made up of small rectangular metal patches close together on a thin dielectric substrate and on the other side of the substrate is the ground plane. The dielectric substrate through the patches of Figure 2.1 is connected to the ground plane.

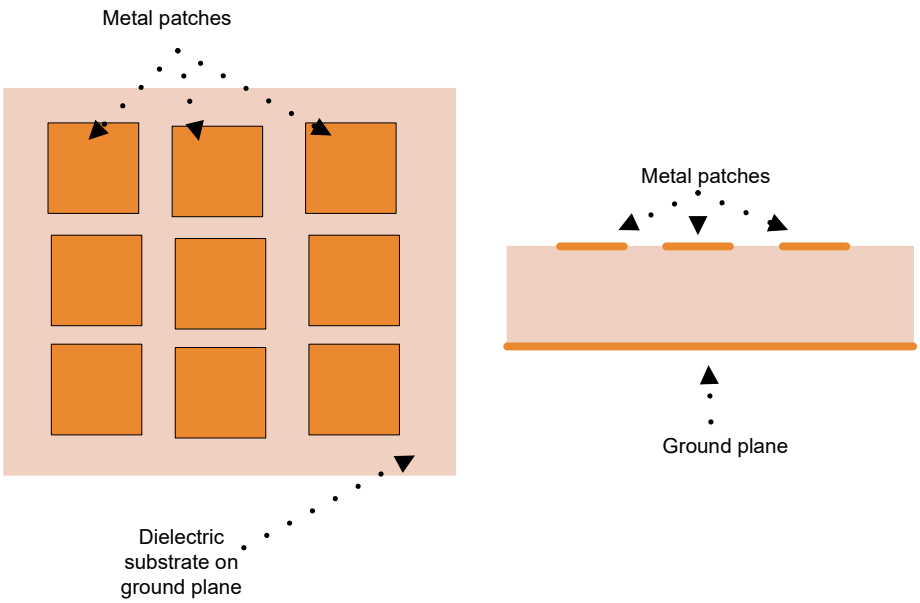

FIGURE 2.1: Top and side view of metasurface structure

With the capability of dynamically tuning the metasurface properties, either to make it conform to a specific input wave or to change its output functionality, many new applications for tunable/reconfigurable metasurfaces were soon found, yielding a great deal of potential [2, 43, 46]. A greater understanding of tunability towards reconfigurable and programmatically controlled metasurfaces arose opportunities to the development of artificial intelligent sheet materials. These can dynamically shape electromagnetic fields, which can have a great impact on imaging, communication, and sensing applications.

2.2 RMS design considerations

In different locations, reconfigurable metasurfaces can be designed to work as reflecting/refracting between the base station and the user, or as waveguide operating at the basestation. They can be passive-lossy, passive-lossless, or active, based on their energy consumption which determines performance capabilities [1]. However, due to their inherent ability to be configured, RMSs cannot be completely passive.

According to authors in [47–49], RMSs are either waveguide, refractive and reflective. The RMS converts and radiates a wave (either induced by an incident wave or fed by a waveguide) into a desired propagating wave in free space. Authors in [47] presented an analysis of waveguide-fed metasurfaces. In their implementation, each of the elements was modeled as an uncoupled magnetic dipole, and its magnitude was proportional to the reference wave and its polarizability. With the metasurface antenna, beamforming can be performed by tuning the polarizability. As a result, every element on a metasurface serves as a micro antenna and by modifying the polarizability, the metasurface antenna can perform beamforming. Compared to conventional antenna arrays, the compact waveguide metasurface occupies less space and transmits a wide range of radiation patterns [47].

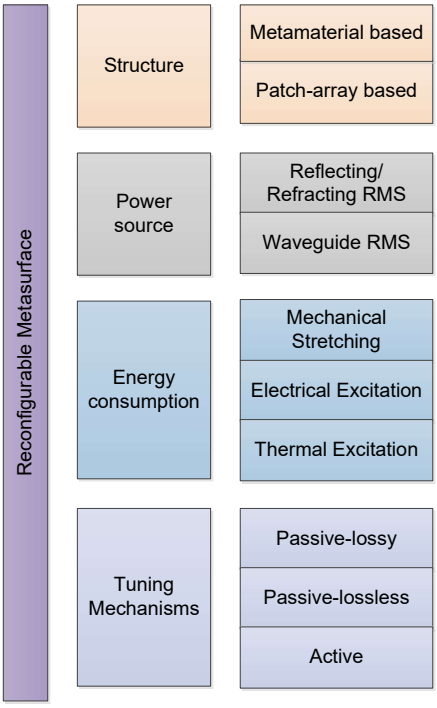

FIGURE 2.2: Parameters to consider when designing RMSs [1]

In [48], theoretically refracting metasurface was designed. In order to optimize the tangential field components at the two sides of the metasurface, the authors used an equivalent impedance matrix model. The authors demonstrated that the passive metasurface can achieve either arbitrary transmission or reflection by using only the

surface electric and magnetic reactance. According to [49], reflecting metasurfaces entails varactor diodes with a tunable bias voltage in each element. Each element can then perform discrete phase shifts and achieve beamforming for the reflected wave by pre-designing several digitized biasing voltage levels. Figure 2.2 gives a brief summary of the different types of RMS. The utilization of reconfigurable metasurfaces as active antennas is a relatively new area of research, in contrast to reflective/refractive metasurfaces that have received considerable attention recently. Additionally, the metasurface antenna leverages the phase advance of the waveguide mode, eliminating the need for phase-shifting circuits that can add cost and complexity to the system [1, 50–53]. Therefore this thesis will focus on waveguide RMSs.

2.3 Implementation of RMS

Metasurfaces can be tuned by adding materials or components (e.g., lumped electronic elements) whose electromagnetic properties can be modulated by external stimuli [20,54]. The way the driving signal is applied depends on the material/element that is being used, such as through a low-frequency electric or magnetic field, through a laser or voltage source, or through changing the ambient temperature [2]. In order to control the electromagnetic response of a metasurface, the externally modulated signal is applied to change its electromagnetic properties such as permittivity or conductivity of a material, which will lead to a modification in the effectivity of the electric and/or magnetic response [55]. There are different physical tuning mechanism employed, such as optical, electro-optical, thermal, magnetic or voltage-based tuning. This section will focus on the aforementioned mechanisms in depth.

2.3.1 Optical Tunable Metasurfaces (OTMs)

The fastest modulation technology involves ultrafast optical pulses, which are highly efficient in creating active metasurfaces in which optically sensitive materials are

used as meta-atoms [43]. Metasurfaces that contain light-sensitive materials can also be made tunable by illumination. It has been shown that semiconductors have conduction carriers (and in turn, dielectric constants) that are greatly influenced by external optical pumping, which is one of the reasons they are commonly used to generate active meta-devices ranging from terahertz (THz) to the visible wavelength range [56, 57]. A photoconductive semiconductor material is a prime candidate for implementing light-tunable metasurfaces, with the most noticeable examples being silicon (Si) and gallium arsenide (GaAs).

In 2006, authors in [58] reported the first OTM, a copper SRR array which was engraved on a semi-insulating GaAs substrate [59]. Under ultrafast (50 fs pulse width) light pumping at 800nm, the authors tested the effect of photoexcitation induced conductivity on metallic SRR gaps, this resulted in a strong modulation on the transmission amplitude at 0.56 THz. The authors concluded that SRR terahertz switches can be turned off by optical excitation, demonstrating their potential. Alternatively, semiconductor materials can also be used to fabricate resonance meta-atom inclusions. The carrier photoexcitation modified the geometry of the resonator: the semiconducting section switched between a dielectric-like and a conductor-like state according to the pump fluency [60]. In addition to SRRs, Si-connected patches were also proposed for transitioning from a cut-wire array (exhibiting Lorentz resonant response) to a wire-grating geometry (exhibiting Drude response) [2].

According to authors [61], the honeycomb-like structure of graphene creates an extraordinary surface with electrical, optical, and mechanical properties as it can be biased by DC gates to change its Fermi level and associated charge carrier density dramatically. By modulating the conductivity, the concentration and distribution of energy within the graphene was altered [62, 63]. Thus, the integration of graphene with passive metasurfaces or structured graphene can improve beam engineering dynamics. A survey by [64] concluded that intensity modulation was the fundamental building block of graphene metasurfaces and over the years, the phase

modulation of waves for wavefront shaping and polarization control has received considerable interest, with a variety of theoretical designs and experimental breakthroughs. Authors in [65] demonstrated THz switching by using graphene as a material and hexagonal metallic meta-atoms as electrodes. The graphene layer with tunable loss provided a surrounding medium for meta-atoms as they worked in the low THz range. By increasing the conductivity of the graphene layer, charge carriers accumulated at the hexagon's edges and leaked into neighboring elements. Due to this, the resonance was weaker and slightly shifted as the biasing voltage was applied from the charge neutral point (CNP) [65]. According to [66,67], a graphene patch or ribbon as a phase shifter will only provide a dynamic phase range of 180° around the plasmonic resonance by varying the Fermi level, which is determined by the Lorentz-shaped electric dipole resonance. In [68–70], graphene metasurfaces with proper biasing voltage, multiple polarization states was switched "ON" and "OFF" in one structure with high modulation speeds, making these devices highly demanding for polarization encoding and multiplexing. Recent years have seen an increase in the use of tunable graphene metasurfaces with optical stimulation. Amongst them are distributed Bragg resonators for lasing and amplification of radiation, parity-time symmetric sensing systems, and a flat magnetic absorber based on graphene with ultrafast modulation [63,71,72].

Voltage-controlled tuning of a lumped element

For microwave applications, tunable lumped electronics, where the output impedance is controlled by a DC voltage signal (biasing), prove an incredibly effective method for realizing tunable metasurfaces. These components have typical characteristics such as variable resistors, PIN switch diodes, and P-N varactor diodes [2]. In order to accomplish tunable metasurfaces, lumped elements are incorporated in the meta-atom configuration and are addressed with proper bias signals.

There are two states of a PIN switch diode, "ON" (conducting) and "OFF" (insulating), which can be accessed by forward bias and reverse bias, respectively. For the "ON" state, PIN diodes are modelled as a series RL circuit and combination of series-parallel RLC circuit for "OFF" state [73]. In [74], a reconfigurable frequency selective surface (RFSS) was designed and implemented, it is a planar periodic structure which consists of basic elements depicted on a dielectric substrate. PIN diodes were incorporated on the metal connection parts of every surface element which were switched "ON" and "OFF" by an external bias [16,75,76]. Most impinging energy passed through the FSS when the bias of the diode was set to reverse bias and its reflected when diode was set to the forward bias. Authors in [2] also incorporated P-N varactor diodes in metasurfaces. Their reactance was adjusted (with relatively small changes in resistance) by altering the reverse bias voltage and vice versa over time. Authors in [77] proposed a metasurface which switched between total absorption and full reflection by adjusting the bias voltage. It was discovered that when the diode is in a state of match (total absorption) or mismatch, the surface impedance of the metasurface changed. In [78], there was a modification of both scattering and polarization properties. During the "ON" state of the diodes, the wave that was impinging on the metasurface was reflected while retaining the same polarization. As a result, the incident wave for an "ON" state was perfectly polarized, but the incident wave for an "OFF" state was lost in transmission. Tunable perfect absorption is one of the most actively investigated functions. Modifying the reverse biasing voltage of the varactors results in a shift of the resonance frequency and, consequently, the spectral position of perfect absorption [79]. According to [2], a few pico Farads (pF) of capacitance (0.5 to 5 pF) were usually required for this purpose and can be achieved with diodes using moderate reverse bias voltages of the order of 0–15 V which are readily available in the market today.

Authors in [80] obtained a reconfigurable system with the use of a varactor-tuned resonator which was programmed in software. In this work, resonant frequency

of available patches was changed by electronically tuning the unit cells instead of modifying resonator dimensions to increase the usable frequency range. A tunable phase shift was attained by modifying the bias voltage applied to the varactor with the intention of evolving its capacity [16]. A tunable capacitor was intergrated with each metasurface unit which allowed EM response of the patch elements to be changed by using micro-controllers [16]. Unlike in [81], authors in [82] controlled a 6×6 transmit-array varactor diodes to investigate its beamforming capabilities at an operating frequency of 5 GHz. A 22×22 reconfigurable metasurface array controlled by PIN switches and varactor diodes operating at 11.5 - 13.5 GHz was implemented by [83] to achieve a 180° phase difference. Although GHz range is mainly the domain for voltage controlled lumped elements, they are the preferred tuning mechanisms for coding and software-defined metasurface implementation.

In [84], the authors examined the dynamic multi-functional properties of a digitally controlled metasurface with a relatively large aperture. The authors demonstrated the dynamic manipulation of EM waves using a programmable metasurface containing 1600 controllable unit cells. Each unit cell contained one PIN diode, allowing for binary coding of an individual polarization to achieve reconfigurable polarization conversation. An inverse fast Fourier transform (IFFT) along with a binary coding matrix and genetic algorithm were then combined and applied to the relatively large metasurface for different scattering and focusing results. The authors then demonstrated directed beams, steering beams, and shaped beams for a point source illumination and confirmed these functionalities via measurements of a practical prototype comprised of five identical sub-metasurfaces controlled via a field programmable gate array (FPGA). Authors in [17] used a a high-speed transmission-type 1-bit coding metasurface to create an essentially broadband transmission-type coding system. This design had multiple layers instead of a single reflection type, which ensured good amplitude transmission, and sufficient phase response without altering incident polarization. The 10-bit states were represented by coding particles

of two types, each with a phase shift of 180 °, between 8.1 and 12.5 GHz. As a result of these coding particles, the authors achieved wideband beamforming function to estimate the performance, in which high-directivity pencil beams were generated in the far field, enhancing the bandwidth characteristic of transmission-type coding metasurfaces [17]. Furthermore, the authors arranged coding particles in the sequence 010101... to radiate two symmetrical deflecting beams in the large range of 30°- 50.5° and thus proving to be more efficient at radiating than conventional leaky-wave metasurfaces. A majority of the designs have been experimentally validated at microwave frequencies in [85,86], with some demonstrations also occurring at THz frequencies [17,87].

In addition, reconfigurable and programmable metasurface functionality can even be further enhanced by converting the actuators (e.g., diodes in typical microwave implementations) into "controllers" with additional functionality. As a result, a smart network of interconnected controllers can sense the impinging wave, communicate with each other, and process information. Through the use of a "gateway" based on standard communication protocols (e.g., wiFi, ethernet, bluetooth), this intra-metasurface communication can be controlled and reconfigured by ordinary people, even by non-specialists [2]. Figure 2.3 illustrates the concept of actuating, sensing, and processing information using software-defined metasurfaces in a networked environment. This concept comprises of one or more metasurface switches which are controlled by a network of miniaturized controllers. As a result of a switch status changing, different switch configurations were dictated, which modified the atom structure of the meta-atom and subsequently altered its electromagnetic functions [88]. Then through a master-slave setup, the input gateway connects the network of controllers with external networking devices.

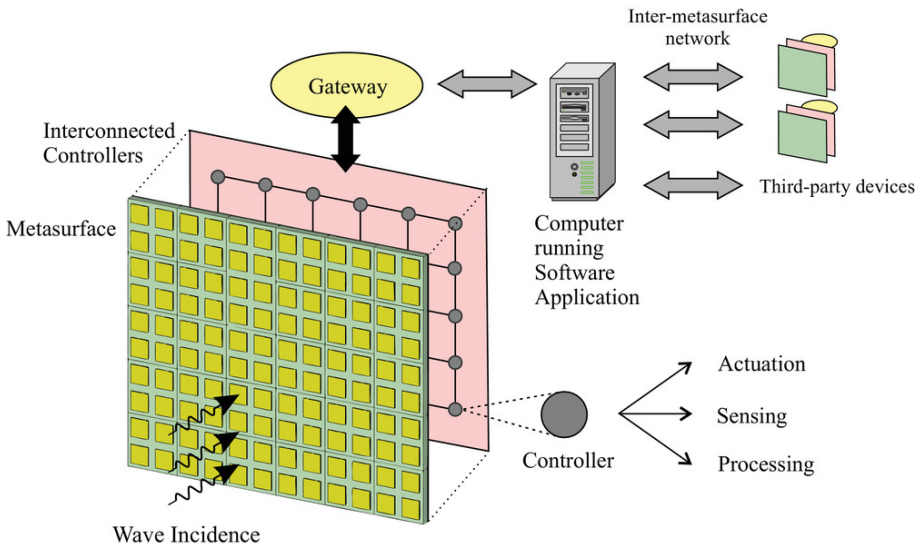

FIGURE 2.3: System concept that combines software-defined metasurfaces with an embedded network of controllers that allows actuation, sensing and processing of information by [2].

Since SDM components are vulnerable to permanent failures, authors in [88] proposed two fault adaptive routing scheme for network controllers. In simulations conducted on a custom-built simulator, the fault adaptiveness of the two algorithms was evaluated based on their success ratios for packet delivery and coverage ratios, i.e., how many nodes are accessible when implementing the routing algorithm. In addition to evaluating the performance characteristics of the two proposed algorithms, the authors simulated the number of message hops any packetized message had to traverse on its way to its destination. On the other hand, authors in [89] developed a wave sensing approach that does not require specialized hardware and instead makes use of the SDM networking capabilities. In this work, nano-networks embedded within the SDM automatically adjusted its energy dissipation to fully absorb the waves, and thus indirectly measuring the attributes of the surface.

Thermal tuning

According to authors in [2], tunable metasurfaces can also be stimulated by heat. Furthermore, materials with strong sensitivity to temperature variations would make the best meta-atoms or substrates for thermally tunable metasurfaces. By utilizing

such sensitivity, the metasurface response can be tuned by observing the electromagnetic change as the temperature varies. When the structural or electronic phase changes across a critical temperature, phase change materials (PCMs) show near-uniform refractive index change [90, 91]. There are at least two phases of PCMs, often referred to as amorphous and crystalline and these occur when the crystal structure of the material changes [92, 93]. While most other materials also exhibit these two phases, PCMs have a unique structure which causes them to have a significant change in refractive index [91]. Silicon dioxide (SiO_2), for example, exists both in the amorphous and crystalline phases, but since they share the same crystal structure, their refractive indices are insignificant [91, 92]. As a result, silicon dioxide is not considered a PCM. In contrast, octahedral amorphous germanium–antimony–telluride/ GeTe–Sb_2Te_3 (GST) transitions to rhombohedral once it becomes crystalline, which results in considerable refractive index changes [94]. Several types of phase change materials such as chalcogenides and transition metal oxides have been used in optical and photonics applications [92].

A chalcogenide is a compound created by combining a chalcogen element (such as sulfur, selenium, tellurium, and polonium) with a metal. GST, a typical chalcogenide PCM, comes in several varieties depending on the concentration of constituent elements, but GST-225 is the most useful as seen in Figure 2.4 [95, 96].

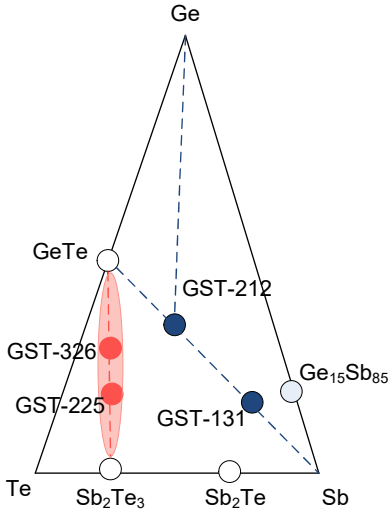

FIGURE 2.4: Ge–Sb–Te phase diagram illustrating important pseudo-binaries

According to authors in [97–99], GST is not the only chalcogenide PCM available; there are also GeTe, Sb_2Te, and $Ag_5In_5Sb_{60}Te_{30}$ (AIST). The crystal structure of these materials exhibits strong resonance bonding, which is why their optical properties differ considerably from those of the material in question [100]. The GST, GSST, Sb_2Te_3 share small electro-negativities, which account for their covalent bonding. At room temperature, both phases are non-volatile, which is advantageous for memory devices, as well as few electronic applications [92, 101].

In [92, 100], authors reviewed some device demonstration using GST, noting that $Ge_2Sb_2Te_5$ are low loss PCMs. Additionally, these PCMs are commonly used due to their fast crystallization speed, large optical contrast, and good reversibility between amorphous and crystalline states [102]. In addition to having advantageous optical properties, GST alloys and other PCMs based on chalcogen have similar chemical properties. The process involves forward crystallization and backward amorphization, which is a reversible process of phase transition. According to authors in [102], the temperature was the determining factor for phase change. Due to this, laser pulses were designed to heat materials above their melting points, but below their crystallization temperatures. The atoms then arranged themselves after slow cooling, as opposed to amorphization, which results in crystalline material. As soon

as the material had reached its melting point, it was rapidly cooled to room temperature to achieve the amorphous state. Due to structural re-arrangement, the electronic densities and transition matrix elements of the two states were different. Aside from the optical properties, the thermal properties are also taken into consideration since $Ge_2Sb_2Te_5$ has thermal conductivities ranging from 0.14 to 1.76 W/(mK) [102,103]. Low thermal conductivity results in less energy being consumed in both crystallization and amorphization, which enhances optical properties [103].

According to authors in [92, 102, 104], transition metal oxides that undergo Mott transition (also known as correlated materials) rank second among PCMs. The conductivity of Mott insulators such as vanadium dioxide (VO_2), is dependent upon temperatures since they transit from insulator to conductor as the temperature rises. VO_2 is a typical example of a PCM showing a metal-to-insulator transition (MIT) with a phase transition temperature of around 68° which is quite close to room temperature [2, 100]. MIT temperatures may be further lowered by compressing the material or by doping it with tungsten [100]. A phase change in VO_2 induced optically also offers a great deal of potential for compact device structures to achieve high speeds and optical modulation. In contrast to using silicon's weak electro-optic properties, VO_2 is easily fabricated on silicon, and its ultrafast switching capabilities can be used to adjust the effective index of ring resonators [105, 106].

Authors in [92] mentioned that modulators and switches can be produced from artificially micro/nanostructured metasurfaces using PCMs. Phase change materials are often present in the microstructures of such devices. Authors in [106] stated that on-chip modulators built from vanadium dioxide have existed for quite a while compared to GST-based devices and they consist of a ring resonator containing a patch of VO_2. When the temperature changes, the phase of VO_2 changes, resulting in a change in resonant frequency.

Magnetic Tuning

Materials and structures that are magnetically responsive have also attracted research interest since they can respond almost instantly, and in a contactless manner, to external magnetic stimuli [2]. In the microwave regime, one of the most well established methods of magnetic tuning involves ferro magnetic resonance (FMR) in ferrite materials such as yttrium iron garnets (YIG) [107, 108]. In the presence of externally applied static or slowly varying magnetic fields, ferrite materials can exhibit Lorentz-type resonance in their effective permeability [2]. As opposed to previous works that focused on electrically tunable metasurfaces, authors in [109] presented a device comprised of ferrite rods and metallic foils that can be made magnetically tunable. They concluded that when the thickness of the ferrite rod and the magnitude of the magnetic field increases, the amplitude and phase of the transmission wave decreases. Also, phase gradient was obtained by tuning the thickness of the ferrite rods as shown in Figure 2.5.

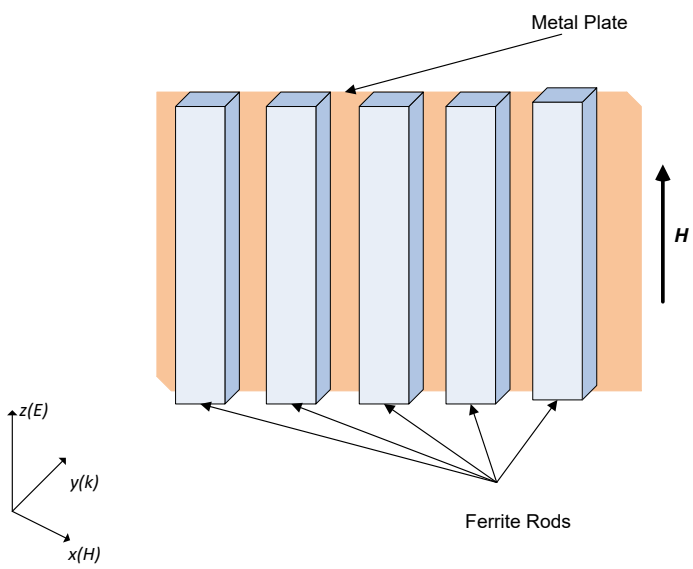

FIGURE 2.5: Schematic diagram of magnetic tunable metasurface

Furthermore, as the rod thickness gradient increased, the metasurface deflection angle increased and deflection angle decreases with increasing magnetic field strength,

which exhibited the property of being magnetically tunable. In [107], a ferrite-dielectric metamaterial composed of dielectric and ferrite cuboids was designed. As a result of applying certain magnetic fields, two resonance frequency dispersion peaks appeared and the effective permittivity peaked. The authors showed that it was possible to adjust the applied magnetic field to tune the metamaterial's permittivity, resulting in a magnetically tunable dielectric property. Authors in [107] presented a new method to fabricate positive refractive index metamaterials, which are more suitable for microwave applications. A study by [108] used a ferrite-based metamaterial structure to prepare tunable metamaterial bandstop filters. From this study, broad bandwidth was obtained by examining the dependence between FMR frequency and ferrite rod size. By adjusting the size of the ferrite metamaterials, the stopband frequency of the designed filter was tuned, which made it suitable for practical applications in tunable microwave devices.

There are a number of metasurfaces that use ferrites as tuning elements, most notably for tunable perfect absorption, with the resonant frequency controlled by an external magnetic field [110, 111].

2.4 Applications of reconfigurable metasurfaces

Research contributions have demonstrated that RMS-enhanced wireless networks are capable of obtaining tuned antenna gains, improved QoS, and enhanced coverage range. In the context of wireless communication, Figure 2.6 illustrates the application of RMSs as either a nearly passive reflective/refractive surface or a waveguide metasurface antenna. From Figure 2.6a, the addition of a reconfigurable metasurface between the user and base station allows the system to overcome non line-of-sight conditions and improve coverage without any power amplification and baseband signal processing [112]. Unlike reflective/refractive RMSs, waveguide RMSs usually act as active antennas at base stations as shown in Figure 2.6b [53].

In the context of wireless communication, reconfigurable metasurfaces are mostly considered passive reflecting devices used to shape the propagation environment [18,113–115]. As an alternative, works in [112,116] presented an application of RMSs as massive MIMO active reconfigurable antennas with developed analog signal processing capabilities for next generation transceivers. The authors further mentioned that the analog beam pattern can be controlled for transmission and reception by tuning the EM properties of the RMS elements. The application leverages their ability to fabricate planar, compact, and low-cost massive antenna arrays that can be used in current and future base stations and access points [116].

According to authors in [117], with higher data rate requirements for RF wireless communications, new types of RF switch matrix multiplexers are needed. Therefore, the authors proposed a reconfigurable metasurface for spatially multiplexing and modulating RF signals. The proposed concept involved feeding multiple data signals into a multiplexing signal matrix to control the phase distribution across the RMS [117, 118]. Phase shift keying (PSK) was performed directly by the metasurface using electronic phase tuning of its individual unit elements. Authors in [118] mentioned that RMS antennas can also perform frequency shift keying (FSK), spatial code modulation (SCM), and spatial shift keying (SSK) signal modulation

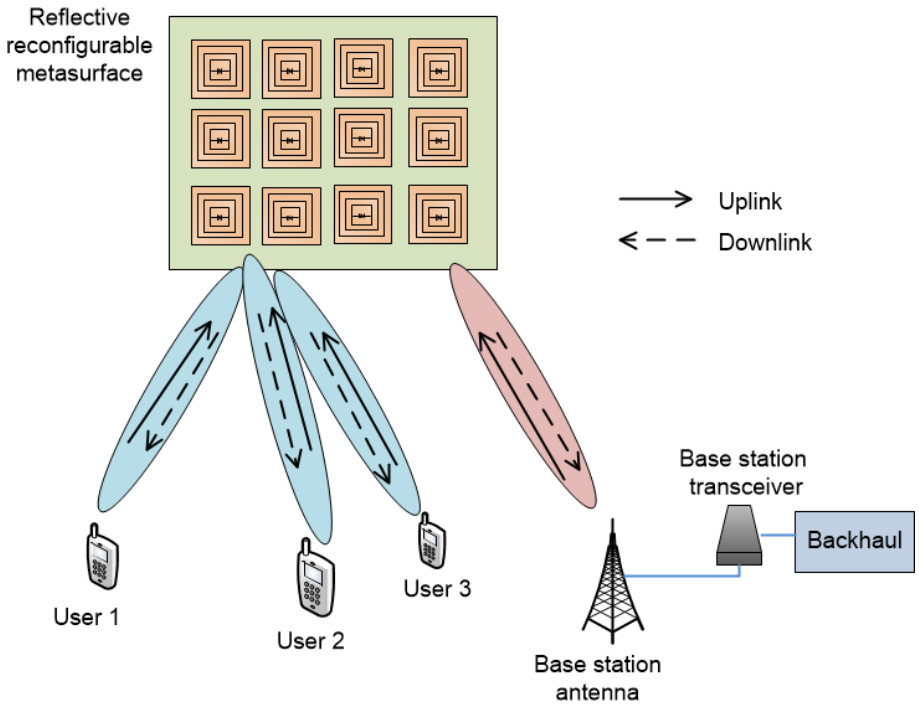

(A) Reflective metasurface

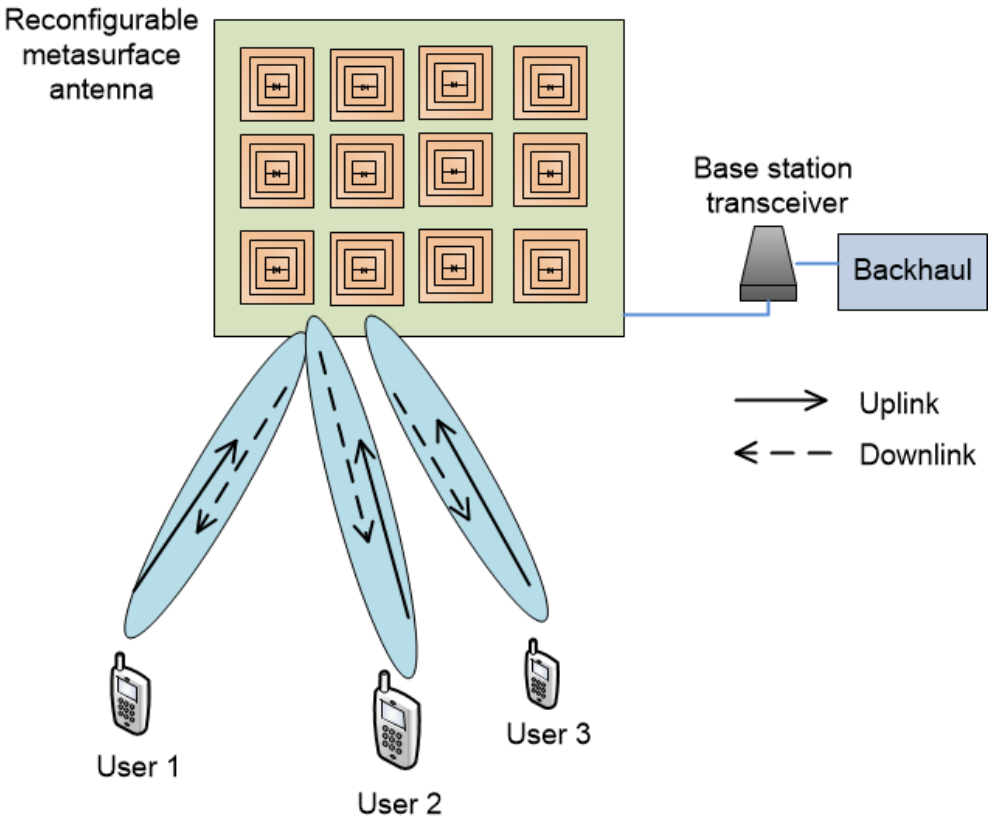

(B) Metasurface antenna

FIGURE 2.6: Two main applications of reconfigurable metasurface.

techniques in addition to PSK.

All mobile devices, climate science, and autonomous vehicles require advanced microwave antennas for imaging, radar, and wireless communication [119,120]. Additionally, antennas rely on electronic beamsteering to function effectively. Therefore, authors in [121] proposed a waveguide-fed RMS structure which enabled electronic beamsteering at 10 GHz. The authors concluded that RMS antennas provide similar performance as conventional array antennas while avoiding phase shifters and amplifiers. Based on this characteristic, the authors further concluded that realistic path towards constellations of satellites can be created for Earth observation and wireless communications [121,122].

The applications of metasurfaces in radar include far-field and near-field systems [118]. Authors in [123] investigated RMS antennas applications for synthetic aperture radar (SAR) in far-fields. The authors concluded that electronically tuned RMSs can generate steerable and directive beams for SAR imaging. As a consequence, the hardware architecture of the SAR system is simplified. In the context near-field applications, RMSs are commonly applied in MIMO radar imaging [124]. Works in [125,126] presented a method for reconstructing images obtained by using a RMS antenna. The authors further demonstrated that range migration algorithms (RMA) could be compatible with the metasurface architecture, which enabled fast Fourier transforms to be used during image reconstruction. The combination of the RMS antenna algorithm could result in a system that was less complex and more efficient.

2.5 Conclusion

From previous works [2,43,46,127], metasurfaces proved to have moved beyond the early demonstrations of fixed, static electromagnetic responses and entered the realm of being tunable, reconfigurable, and programmable. In tunable metasurfaces, the electromagnetic waves were manipulated without changing the physical

structure of the elements. The implementation of reconfigurable metasurfaces depends on the frequency of operation; tuning schemes, design strategies, and the limitations change with each frequency regime. The applications of RMSs are dependent on whether they are designed as passive reflective/refractive surfaces or active waveguide metasurface antennas. As a passive reflective/refractive surface, RMSs are placed between the user and base station to allow the system to overcome non line-of-sight conditions and improve coverage without any power amplification and baseband signal processing. Unlike reflective/refractive RMSs, waveguide RMSs usually act as active antennas at base stations.

In comparison with the conventional phased array or electrical scanned antennas, RMS antennas have the ability to provide comparable performance with extreme low cost and complexity [112, 121].

Chapter 3

Design Procedure of Metasurface Unit Cell

The previous chapters highlighted on ways to implement RMSs. Further areas of application were discussed. Reconfigurable metasurfaces are made from SRRs, therefore this chapter introduces the existing design procedure of a square and circular shaped SRR.

3.1 Introduction and Related Works

There is a new paradigm in modern science with the rise of metamaterials and in particular left-handed metamaterials, which enable development of new microwave components with advantageous properties. Metamaterials are designed using split ring resonators as a structure to produce the desired magnetic response to an applied EMF [128–132]. The split ring is a basic geometry for designing sub-wavelength magnetic metamaterial resonators. It typically consists of two metal rings that are either square or circular, etched or carved onto dielectric materials as shown in Figure 3.1 [128]. Both geometries from the figure have a copper strip width w and spacing between the rings d. The gaps between the inner and outer rings are denoted by g_1 and g_1, respectively. When magnetic fields are applied, an electromotive force that induces currents that flow from one ring to another ring through the gaps g_1 and

g_2 is created. Consequently, the structure behaves as an LC circuit with resonance frequency f_o.

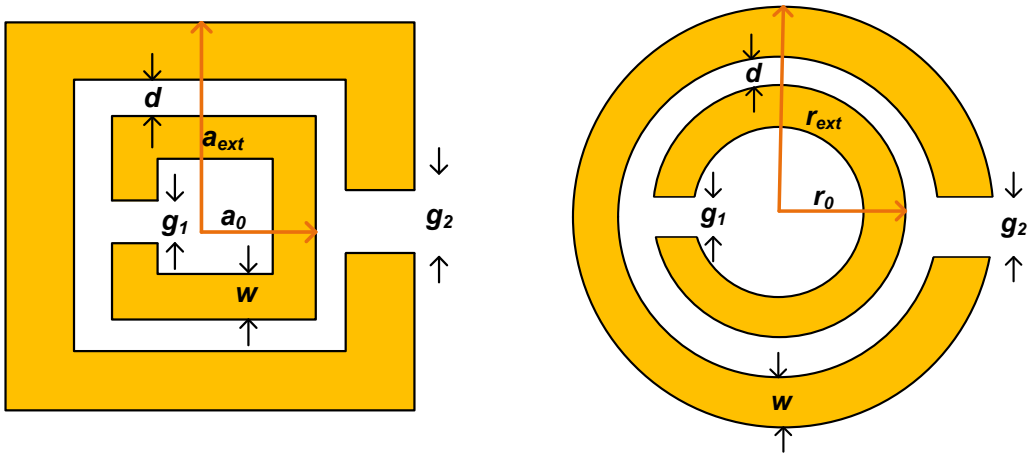

(A) Square (B) Circular

FIGURE 3.1: Geometry of SRR

Authors in [133] proposed an analytical model for predicting the charge and potential distributions in the fundamental mode of a 3D SRR with square cross section. In this model, the authors derived the equivalent capacitance formulae and resonance properties was determined at any frequency. Authors in [134] designed and experimentally validated a square co-planar waveguide with stop band characteristics for filter applications. Its small size made it more suitable for applications at lower microwave frequencies. They presented a simplified formulation for estimating the resonant frequency of the employed square SRR. They further concluded that this formulation can be used to design SRRs for obtaining precise stop bands in co-planar waveguides and similar applications. In [135], the authors analyzed the SRR of different geometrical shapes (i.e square, circular and hexagonal) using simple equivalent circuits. The authors concluded that circular SRRs resonate at higher frequencies than square SRRs, despite having similar dimensional parameters. Additionally, there was a comparison between the various split ring resonator shapes, including circular, square, hexagonal, and triangular in [136] for energy harvesting applications. Authors in [137] exploited the symmetry properties of split

ring resonators to implement novel sensing devices. It consisted of a co-planar waveguide that had movable SRRs attached to its back surface. The authors concluded that between circular and square shaped SRRs, the square geometry was necessary to enhance the sensitivity of the structures. Additionally in [138], the authors developed novel printed microwave elements based on square and circular SRRs. They concluded that as an alternative to originally proposed circular SRRs, square shaped ones can be used to enhance coupling of the structures. In [139], the comparative analysis between the two geometries showed that the square SRR yielded more bandwidth than the circular one. The square shaped structure is the most commonly studied variant of SRR since it has more design flexibility.

In previous literature, once relevant inductances and capacitances were known, the resonant frequency of the SRR which depended on its geometrical parameters was determined [140–]. Despite this, a complete theoretical formulation of the SRR unit cell dimensions was not presented. Authors in [147] employed the simple analytical model for SRR in order to obtain preliminary line guides for the actual design, which was numerically performed via Computer Simulation Technology Microwave Studio (CST MWS). The geometry of the SRR unit cell and cell size were parametrically changed using the mentioned EM solver in order to operate at intended frequency of operation. In [148], the authors constructed a structure consisting of two G-shaped SRRs linked together. Furthermore, the effects of unit cell size on the resonance frequencies of a metamaterial were examined for four different unit cells with different design parameters. However, the formulation of achieving SRR geometries was not presented.

3.2 Theoretical formulation

Figure 3.2 shows the equivalent circuit of both the square and circular shaped SRR from Figure 3.1. From Figure 3.2, the metallic rings contribute a total inductance of L_T and distributed capacitances of C_1 and C_2 in the top and bottom halves of the

SRR structure, respectively [128]. Additionally, the equivalent circuit includes the gap capacitances, C_{g1} and C_{g2}, that occur when the rings are split.

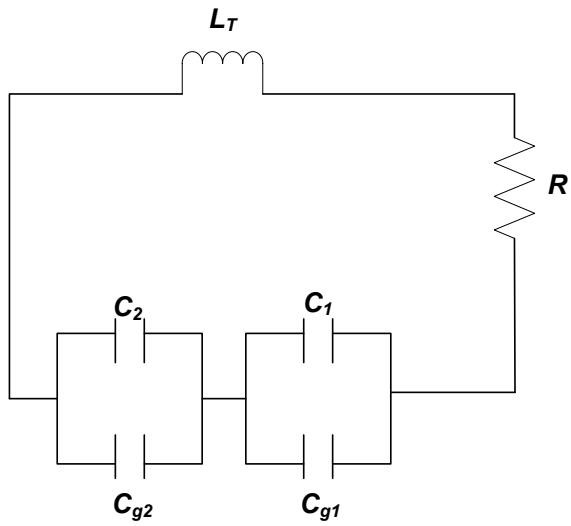

FIGURE 3.2: Equivalent circuit with gap capacitances taken into account

In the square SRR, the resonant frequency is given by [135]

$$f_o = \frac{w_o}{2\pi} = \frac{1}{2\pi}\sqrt{\frac{1}{L_T C_{\text{eq}}}}, \tag{3.1}$$

where ω_o is angular velocity and C_{eq} is the total equivalent capacitance of the structure which is evaluated as

$$C_{\text{eq}} = \frac{(C_1 + C_{g1})(C_2 + C_{g2})}{(C_1 + C_{g1}) + (C_2 + C_{g2})}. \tag{3.2}$$

Due to the identical gap dimensions $g_1 = g_2 = g$, gap capacitances $C_{g1} = C_{g2} = C_g$ and the series capacitances $C_1 = C_2 = C_0$, equation 3.2 can be modified as [149],

$$C_{\text{eq}} = \frac{(C_0 + C_g)^2}{2(C_0 + C_g)}. \tag{3.3}$$

The gap capacitances of strip conductors based on a metal thickness t can be represented as

$$C_g = \frac{\epsilon_0 \mathrm{w} t}{g}, \tag{3.4}$$

where, ϵ_0, w and t represent the free space permittivity, width and thickness of the metallic rings. As mentioned previously, the distributed capacitances C_0 are dependent on the split gap dimensions g, the capacitance per unit length C_{pul}, the square average ring radius a_{avg} therefore for a square SRR it is defined as,

$$C_0 = C_1 = C_2 = 4a_{\mathrm{avg}}C_{\mathrm{pul}} - gC_{\mathrm{pul}}, \tag{3.5}$$

where,

$$a_{\mathrm{avg}} = a_{\mathrm{ext}} - \mathrm{w} - \frac{d}{2}. \tag{3.6}$$

The radii is denoted by a_{ext} as shown in Figure 3.1a. The capacitance per unit length is defined as

$$C_{\mathrm{pul}} = \frac{\sqrt{\epsilon_e}}{cZ_0}, \tag{3.7}$$

where

- c - velocity of light in free space
- ϵ_e - effective permittivity of the medium
- Z_0 - characteristic impedance of the line.

For a circular shape shown in Figure 3.1b, equation (3.5) is given as

$$C_0 = C_1 = C_2 = \pi r_{\mathrm{avg}}C_{\mathrm{pul}} - gC_{\mathrm{pul}}, \tag{3.8}$$

where the circular ring average r_{avg} is dependent on the the distance of the rings from the centre r_{ext} of the circular geometry and is defined as

$$r_{\mathrm{avg}} = r_{\mathrm{ext}} - \mathrm{w} - \frac{d}{2}. \tag{3.9}$$

The effective permittivity can be calculated as [150, 151]

$$\epsilon_e = 1 + \frac{(\epsilon_r - 1)}{(2)} \frac{(K(k')K(k_1))}{K(k)K(k_1')}, \tag{3.10}$$

where k is the elliptic modulus and is defined as,

$$k = \frac{\mathrm{w}/2}{(\mathrm{w}/2) + 2d}, \tag{3.11}$$

k′ the complementary modulus which is given as

$$k' = \sqrt{1 - k^2}, \tag{3.12}$$

and $K(k)$ is a complete elliptic function of the first kind and $K(k')$ is its complimentary function. From equation (3.11), the nominator and denominator can be represented by a and b respectively to give

$$k_1 = \frac{\sinh(\pi a/2h)}{\sinh(\pi b/2h)}. \tag{3.13}$$

Equation (3.14) represents the approximate expression for $K(k)/K(k')$ as

$$\frac{K(k)}{K(k')} = \begin{cases} \left[\frac{1}{\pi} ln\left(2\frac{1+\sqrt{k'}}{1-\sqrt{k'}}\right)\right]^{-1} & \text{for} \quad 0 \leq k \leq 0.7 \\ \frac{1}{\pi} ln\left(2\frac{1+\sqrt{k'}}{1-\sqrt{k'}}\right) & \text{for} \quad 0.7 \leq k \leq 1. \end{cases} . \tag{3.14}$$

The characteristic impedance from equation (3.7) is then calculated as

$$Z_0 = \frac{120\pi}{\sqrt{\epsilon_e}} \frac{K(k)}{K(k')}. \tag{3.15}$$

Substituting the values of C_0 and C_g in equation (3.3) for each geometry gives the equivalent capacitances of circular shape C_{eqc} and square shape C_{eqs} as follows

$$\begin{aligned} C_{eqs} &= \left(2a_{avg} - \frac{g}{2}\right)C_{pul} + \frac{\epsilon_0 wh}{2g}, \\ C_{eqc} &= \left(\frac{\pi r_{avg} - g}{2}\right)C_{pul} + \frac{\epsilon_0 wh}{2g}. \end{aligned} \tag{3.16}$$

Therefore, the resonant frequency in equation (3.1) for different SRR geometries was represented as

for square SRR:

$$f_o = \frac{1}{2\pi\sqrt{L_T\left[\left(\frac{4a_{avg}-g}{2}\right)C_{pul} + \frac{\epsilon_0 wh}{2g}\right]}}, \tag{3.17}$$

for circular SRR

$$f_o = \frac{1}{2\pi\sqrt{L_T\left[\left(\frac{\pi r_{avg}-g}{2}\right)C_{pul} + \frac{\epsilon_0 wh}{2g}\right]}}. \tag{3.18}$$

The simplified formula for evaluating the total equivalent inductance L_T for a rectangular wire is formulated as [152]

$$L_T = 0.0002l\left(2.303\log_{10}\left(\frac{4l}{t_o} - \gamma\right)\right)\mu H, \tag{3.19}$$

where l and t_o are the finite length and thickness of a wire. The constant γ is 2.853 and 2.51 for a wire loop of square and circular geometries respectively. The finite length represented as l_s for square SRR and l_c for circular geometry can be determined as follows:

$$l_s = 8a_{ext} - g, \tag{3.20}$$

$$l_c = 2\pi r_{ext} - g. \tag{3.21}$$

Authors in [153, 154] presented a design approach on how to calculate the SRR geometrical parameters. For a circular SRR depicted in Figure 3.1b, the external and internal resonance frequencies defined by f_{c1} and f_{c2} respectively were determined by

$$f_{c1} = \frac{c}{2R_{\text{ext}}\sqrt{\epsilon_{\text{eff}}}}, \quad f_{c2} = \frac{c}{2R_0\sqrt{\epsilon_{\text{eff}}}}, \tag{3.22}$$

$$R_{\text{ext}} = 2\pi r_{\text{ext}} - g_2 - 4\text{w}, \quad R_0 = 2\pi r_0 - g_1 - 4\text{w}, \tag{3.23}$$

where w is the width and g_1 and g_2 represent the internal and external gaps of the rings respectively. R_{ext} and R_0 represents the average radius length of each ring, r_{ext} and r_0 represents the external and internal mean radius length respectively. The effective dielectric constant was represented by ϵ_{eff}, Similarly, for the square SRR shown in Figure 3.1a, the resonance frequency was calculated as

$$f_{s1} = \frac{c}{2L_1\sqrt{\epsilon_{\text{eff}}}}, \quad f_{s2} = \frac{c}{2L_2\sqrt{\epsilon_{\text{eff}}}}, \tag{3.24}$$

$$L_1 = 4l_1 - g_1 - 4\text{w}, \quad L_2 = 2l_2 - g_2 - 4\text{w}, \tag{3.25}$$

where f_{s1} and f_{s2} defined the external and internal resonance frequencies respectively. The average length of each ring was depicted as L_1 and L_2 and the external and internal side length were represented as l_1 and l_2 respectively.

3.3 Conclusion

This chapter has demonstrated the existing theoretical analysis of designing a square and circular split ring resonators. Metamaterials are designed using SRRs as a structure to produce the desired magnetic response to an applied EMF. SRRs typically consists of two metal rings that are either square or circular, etched or carved onto dielectric materials. By using the closed form expression derived in equation (3.2), a design engineer can determine the resonance frequency of SRRs affecting the split gap dimension. In the cases this method has been applied from literature, there

has not been an explicit method on how the average lengths, external and internal side lengths of both circular and square shaped SRRs were calculated. Therefore, Chapter 4 proposes a method to show how every SRR geometrical dimension is calculated in order to present a unified step-by-step procedure. From literature, it can be concluded that the square shaped SRR produced more bandwidth and less reflection . Additionally it has more degrees of freedom from the design aspect than circular ones. Hence why the square SRR will be evaluated for the proposed design in the next chapter.

Chapter 4

Design Procedure of a Frequency Reconfigurable Metasurface Antenna at mmWave Band

In this chapter, a step-by-step method for demonstrating the design of a metasurface antenna is presented. The method is further used to design a frequency reconfigurable metasurface antenna for mmWave applications at 28 GHz and 40 GHz.

4.1 Introduction

The under utilized mmWave spectrum has given an opportunity to researchers to investigate and exploit this band with the aim to curb issues on bandwidth and channel capacity associated with 5G and 6G [155]. A new era in wireless communication has begun with the emergence of millimeter waves utilization and further exploration of sub-mmWaves as the need for higher data rates grows [4,156]. However, high frequencies introduce high pathloss, which results in the need to increase antenna gain requirements [156]. Authors in [54, 84] mentioned that pathloss and multipath fading effects can be mitigated with the use of metasurfaces. A revolution in electromagnetic manipulation has taken place through the use of metamaterials and metasurfaces.

Metasurfaces are 2D arrays of engineered meta-atoms resembling metamaterials which are used to control or modify various parameters, such as amplitude, phase, polarization. They are based on resonant unit cells with a narrow bandwidth around a fixed working frequency [157]. In particular, reconfigurable metasurfaces are of great interest to scientists. RMSs involve adding tunability to each unit cell which allows for more capabilities of metasurface applications. Furthermore, integrating electronic components or tunable materials such as, micro electromechanical systems (MEMS) switches, PIN diodes, liquid crystal or piezoelectric materials, and varactor diodes enables reconfigurability to the metasurface structure [158]. MEMS switches have recently gained attention because of their small size and linearity, but, when compared to PIN diodes, they have a relatively slow switching time [159]. RMS applications using PIN diodes are capable of operating at up to 60 GHz, as well as at low cost, low control voltage and high reliability [160]. It is impossible to use switches in applications requiring a continuous phase change due to their discrete nature. Liquid crystal can change the dielectric coefficient of a unit cell by tens of percent and can be fabricated in its surface without external elements [161]. Due to its physical size changes, the piezoelectric method exhibits limited flexibility, which is also a disadvantage [162]. Researchers are more interested in electrically reconfigurable metasurfaces, since they are less complex and easier to fabricate. Therefore PIN and varactor diodes are most commonly used to achieve reconfigurable electronic tuning.

Multiple applications have been developed for RMSs, such as increasing antenna gain, bandwidth and efficiency [8, 163]. They are even used to design reconfigurable antennas [164]. In order to improve performance of communication systems in terms of interference reduction, power consumption, and system security, it is necessary to reconfigure the radiation pattern of the antennas [8]. With significantly improved cost and manufacturing efficiency, metasurface antennas are emerging as

an alternative to conventional electronic scanned antennas [47, 119, 165]. Metasurface antennas have been found to offer a number of advantages in terms of weight and power consumption over conventional antennas, particularly in security screening, satellite communication, and earth observation applications [166]. Therefore, this chapter proposes a unified simple design procedure used in antennas to calculate the geometrical parameters of SRRs which are used in metasurface unit cells. The proposed unit cell is further used to design a PIN diode based reconfigurable metasurface antenna for the realization of dual band operation at mmWave frequencies.

4.1.1 Related Works

Several researchers have reported various RMSs in the last decade [2,43,83,129,167–172]. Works in [129] proposed a reconfigurable metasurface antenna based on a PIN diode for beam switching applications. The authors proposed a metasurface consisting of periodic double-SRR whose fundamental resonant frequency could easily be controlled by their respective dimensions. Based on their simulations and experiments, the proposed metasurface antenna had good impedance matching and moderate gain performance of about 6 dBi across the band of interest. In [173], the authors presented a dynamically reconfigurable holographic metasurface antenna for applications in near-field beam focusing. Through the use of the proposed metasurface antenna, the authors achieved beam-focusing without requiring phase shifters and power amplifiers. The concluded that the proposed metasurface antenna was suitable for applications that require dynamic reconfigurability, such as imaging and wireless power transfer.

Works in [170, 174] presented a reconfigurable metasurface antenna that manipulated scattering fields by liquid metal. The reflected element phase responses underwent distinct phase differences when the metal shape of the metasurface element changed along the polarization direction. It was concluded that the liquid-metal

metasurface antenna presented had less system complexity, lower cost, and much lower power consumption. In [175], a frequency reconfigurable dielectric resonator antenna using metasurfaces was proposed. The attained bandwidth and gain of the proposed metasurface antenna was 1.1 GHz and 7.8 dBi respectively. However, there was minimal clarity regarding the geometrical parameters of the metasurface unit cells in these previous works.

4.1.2 Contribution

In literature, the design of SRR geometrical parameters were shown. However, previous design approaches lacked clarity on calculating all the geometries of an SRR. The focus of this chapter is to present a unified design framework to calculate the geometrical parameters of an SRR to be used for reconfigurability at mmWave bands. The main contributions of this chapter are summarized as follows:

- Firstly, a demonstration of a step-by-step procedure on how to achieve split ring resonators geometrical parameters at dual frequency of operation is provided.
- Secondly, the proposed unit cell was used to design a 16 element frequency RMS.
- Finally, the characteristics of the proposed frequency RMS were analyzed and compared with previous works.

4.2 Proposed Methodology

According to [176], ring resonators are described as two identical half guided wavelength ($\lambda_g/2$) which establish standing waves in parallel. Figure 4.1 depicts a schematic view of the dual band square SRR structure.

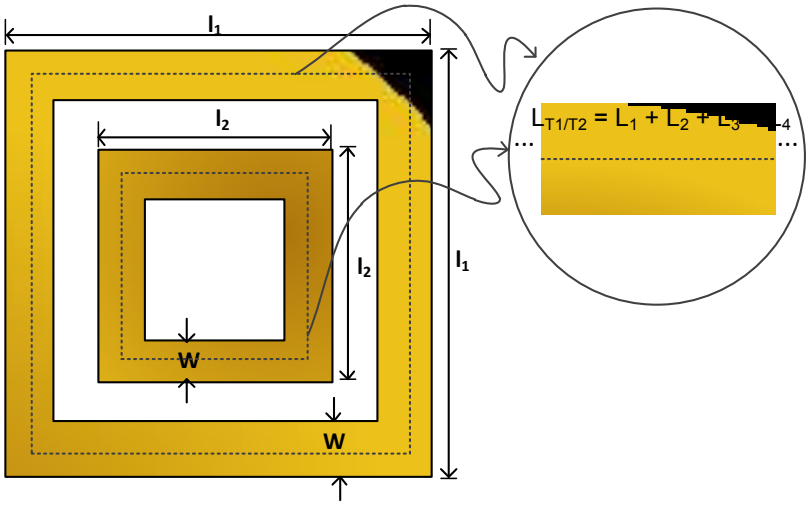

(A) Top View

(B) Perspective view

FIGURE 4.1: Proposed metasurface unit cell

Since L_{T1} and L_{T2} in Figure 4.1 represents the total path transversed by EM waves in the internal and external ring respectively, the fundamental mode length $\lambda_g/2$ is represented as,

$$L_{\mathrm{T1}} = \frac{\lambda_g}{2}, \quad L_{\mathrm{T2}} = \frac{\lambda_g}{2}. \tag{4.1}$$

The guided wavelength at resonant frequency f_o is represented by the following equation [176]

$$\lambda_g = \frac{\lambda_o}{\sqrt{\epsilon_{\mathrm{eff}}}} = \frac{c}{f_o\sqrt{\epsilon_{\mathrm{eff}}}}, \tag{4.2}$$

therefore, the internal and external ring guided wavelengths λ_{g1} and λ_{g2} respectively are given as

$$\lambda_{g1} = \frac{c}{f_1\sqrt{\epsilon_{\mathrm{eff}}}}, \quad \lambda_{g2} = \frac{c}{f_2\sqrt{\epsilon_{\mathrm{eff}}}}, \tag{4.3}$$

where resonance frequencies of the internal and external rings are defined by f_1 and f_2 respectively. The effective dielectric constant is calculated as [177]

$$\epsilon_{\text{eff}} = \frac{\epsilon_r + 1}{2} + \frac{\epsilon_r - 1}{2}\left[1 + \frac{12h}{W}\right]^{-1/2} \qquad \text{for} \quad \frac{W}{h} > 1, \tag{4.4}$$

where ϵ_r represents the dielectric constant. To attain the internal and external ring average length at any specified resonant frequency, equation (4.3) is substituted into equation (4.1) to give [176]

$$L_{T1} = \frac{c}{2f_1\sqrt{\epsilon_{\text{eff}}}}, \quad L_{T2} = \frac{c}{2f_2\sqrt{\epsilon_{\text{eff}}}}. \tag{4.5}$$

Furthermore, since resonators exhibit the same standing waves at fundamental modes, equation (4.5) is used for both one-port and two-port resonators [176].

From the specified substrate information, the dielectric constant ϵ_r and height h are used to calculate the width W of the ring resonator. For a given characteristic impedance Z_o, the width is represented as;

$$W = \begin{cases} \frac{8e^A}{e^{2A}-2}h & \text{for} \quad \frac{W}{h} < 2, \\ \frac{2}{\pi}\left[B - 1 - \ln(2B-1) + \frac{\epsilon_r - 1}{2\epsilon_r}\left(\ln(B-1) + 0.39 - \frac{0.61}{\epsilon_r}\right)\right]h & \text{for} \quad \frac{W}{h} > 2, \end{cases} . \tag{4.6}$$

where

$$A = \frac{Z_o}{60}\sqrt{\frac{\epsilon_r + 1}{2}} + \frac{\epsilon_r - 1}{\epsilon_r + 1}\left(0.23 + \frac{0.11}{\epsilon_r}\right),$$
$$B = \frac{377\pi}{2Z_o\sqrt{\epsilon_r}}.$$

From equation 4.5, the internal and external side lengths l_1 and l_2 of each ring of the SRR can be calculated by,

$$l_1 = L_{T1} + \frac{W}{2}, \quad l_2 = L_{T2} + \frac{W}{2}. \tag{4.7}$$

The permittivity and permeability are calculated from the refractive index (η) and impedance values z using equations (4.8) and (4.9) in order to confirm if the designed SRR represents a double negative metamaterial.

$$\epsilon = \frac{\eta}{z}, \tag{4.8}$$

$$\mu = \eta z, \tag{4.9}$$

where η and z are denoted as [153, 178]

$$\eta = \frac{1}{kl}\Re\{\ln(e^{jnkl_{\text{out}}})\} - \Im\{\ln(e^{jnkl_{\text{out}}})\}, \tag{4.10}$$

$$z = \frac{(1+S_{11}^2)^2 - S_{21}^2}{(1-S_{11}^2)^2 - S_{21}^2}. \tag{4.11}$$

From equations (4.10) and (4.11), the reflection and transmission coefficients are represented by S_{11}^2 and S_{21}^2 respectively, $\Re\{\cdot\}$ and $\Im\{\cdot\}$ denotes real and imaginary components, k represents the wave number and $e^{jnkl_{\text{out}}}$ is represented as [179]:

$$e^{jnkl_{\text{out}}} = \frac{S_{21}^2}{1 - S_{11}\left(\frac{z-1}{z+1}\right)}. \tag{4.12}$$

4.3 Simulation Processes

With the foregoing mathematical analysis, a practical square split ring resonator was designed using CST MWS software. The MWS is based on solving Maxwell's equations in differential form in the time domain explicitly [180]. Additionally, it is highly desirable to use time domain simulations methods for high frequency electromagnetic applications, especially when broadband results are desired [181]. In this work, a square SRR resonating at 28 GHz and 40 GHz was constructed on an RT5880 substrate with height of 0.5 mm as depicted in Figure 4.1. The metallic layer used was the lossy annealed copper. The desired dimensions were obtained by using design equations discussed in Section 4.2 and a summary of a step-by-step

design procedure is shown in Table 4.1.

TABLE 4.1: Summary of calculation of dimensions of a metasurface unit cell

Step	Equation	Purpose
1	Equation (4.6)	Calculate the width of a characteristic impedance Z_o.
2	Equation (4.5) and (4.12)	Calculate the dielectric constant and use it to find the internal and external average lengths L_{T1} and L_{T2} for each frequency.
3	Equation (4.7)	Calculate the internal and external side lengths of each outer ring using the calculated average lengths in Step 2.

Following the use of the design procedure, in order to optimize the calculated parameters of the unit cell of the metasurface, the CST optimizer tool from the software was used. Table 4.2 depicts the dimensions of the unit cell before and after optimization.

TABLE 4.2: Unit cell dimensions before and after software optimization

Dimensions	Before optimization (mm)	After optimization (mm)
h	0.5	0.56
W	1.54	1.54
l_1	3.51	3.47
l_2	4.68	4.4

In order to perform simulation in CST MWS, boundary conditions have to be defined. For the software to generate EM waves, the boundary conditions of the x_{axis}, y_{axis} and z_{axis} were defined as a perfect electric conductor, perfect magnetic conductor and open respectively. This means that for x_{min} and x_{max} the magnetic fluxes are

set to zero, for y_{min} and y_{max} electric fluxes are set to zero and with z_{min} and z_{max} waves can pass with minimal reflections. The proposed structure was excited by defining two wave ports which were normal to the x_{axis}. The time domain solver which comprises of finite difference time domain (FDTD) was used to calculate transmission of energy between excitation sources and obtain broadband frequency behaviour of the simulated structure.

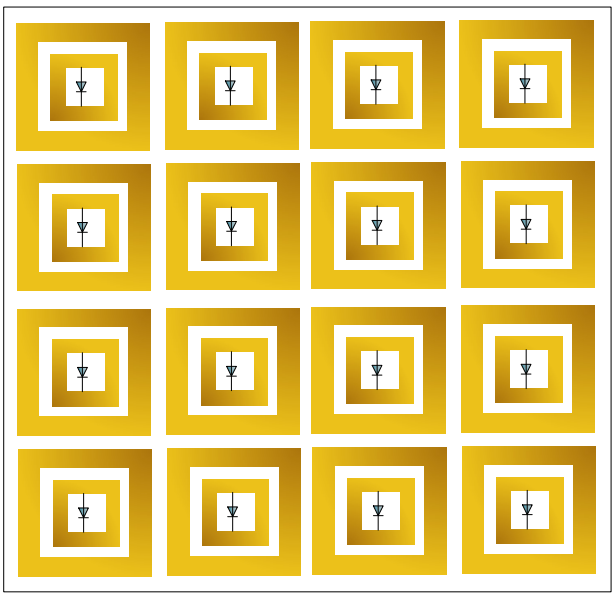

FIGURE 4.2: A 4×4 RMS integrated with PIN diodes

To achieve reconfigurability, the designed unit cell was made into a 4×4 element integrated with diodes as shown in Figure 4.2. Similar to authors in [84], each unit cell of the metasurface was connected to a diode.

4.4 Results and Analysis

As a result of the computations from CST MWS, optimized dimensions, return loss curves, reflection phase, gain, directivity, effective permittivity and permeability of the proposed frequency RMS were analyzed in this section.

4.4.1 Reflection Coefficient

For resonant frequencies of 28 GHz and 40 GHz, a reflection coefficient/return loss graph which shows the ratio of the amplitude of the reflected wave to the incident wave was simulated, yielding the results shown in Figure 4.3. As seen from the figure, before optimization, the unit cell resonated at 25.6 GHz and 39.85 GHz with a magnitude of -14.80 dB and -13.11 dB respectively. With the use of CST optimizer, the unit cell resonated at 28.3 Ghz and 40.3 GHz with a reflection coefficient of -18.57 dB and -22.0 dB respectively. The bandwidth of the unit cell before optimization was 4.65 GHz and 0.67 GHz and after optimization as depicted at the -10 dB mark in Figure 4.3 it was 6.8 GHz and 1.50 GHz. When the unit cell was optimized, it resonated at a frequency closer to the desired operating frequencies (i.e, 28 GHz and 40 GHz) with less reflection than before. As a result, the optimized return loss results of the unit cell were used to analyze a 4×4 frequency RMS antenna structure shown in Figure 4.2. The student version simulation software was not licensed for hundreds of elements, therefore an array characterized by 16 elements was chosen.

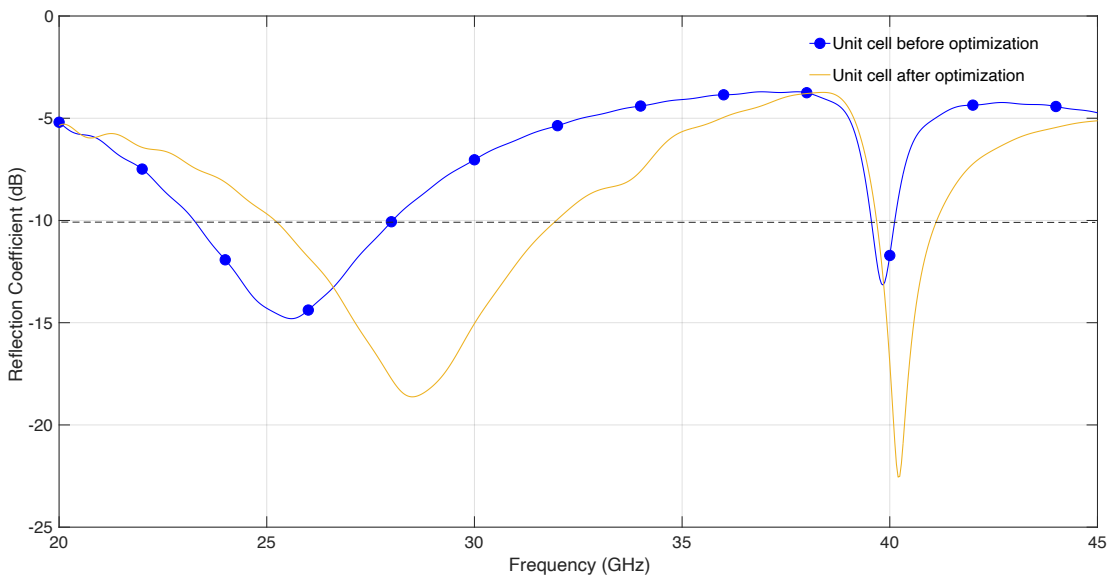

FIGURE 4.3: Return loss results of metasurface unit cell before and after optimization

Figure 4.4 depicts return loss results for a 4×4 metasurface antenna with and without adding PIN diodes from the lumped elements section in CST MWS which enable frequency reconfigurability. The results are further numerically summarized in Table 4.3. It was observed that when diodes were added, resonating frequency decreased as the capacitance increased. From the table, the bandwidth of the 16 element metasurface antenna without diodes was relatively the same as when they were added. Furthermore, it can be observed from this table and figure that the proposed metasurface antenna array was capable of frequency reconfiguration.

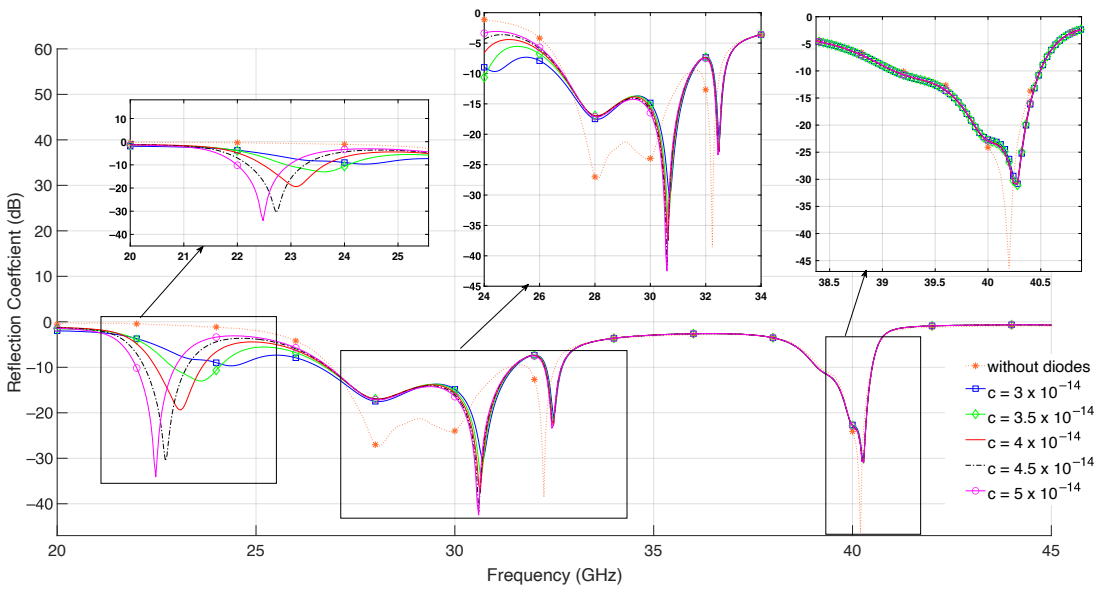

FIGURE 4.4: Return loss simulation results of 16 element metasurface array with and without PIN diodes.

shows a summary of its return loss and bandwidths at different capacitances.

TABLE 4.3: Summary of return loss and bandwidth results

Capacitance (pF)	Resonating frequency (GHz)	Bandwidth (GHz)
Without diodes	26.90 - 31.39, 32.26 and 40.20	4.46, 0.66 and 1.36
0.03	26.61 - 31.49, 32.49 and 40.28	4.88, 0.42 and 1.41

Capacitance (pF)	Resonating frequency (GHz)	Bandwidth (GHz)
0.035	23.60, 26.72 - 31.47, 32.48 and 40.28	1.17, 4.73, 0.43 and 1.41
0.04	23.08, 26.79 - 31.46, 32.48 and 40.24	1.17, 4.68, 0.44 and 1.39
0.045	22.72, 26.81 - 31.44, 32.48 and 40.24	1.05, 4.63, 0.45 and 1.38
0.05	22.48, 26.89 - 31.43, 32.44 and 40.24	0.98, 4.58, 0.46 and 1.38

4.4.2 Reflection Phase

Figure 4.5 shows the reflection phase for the proposed 16 elements metasurface antenna with and without PIN diodes. As observed from the figure, there was a phase difference of 21.8° and 4.3° at 28 GHz and 40 GHz (designed operating frequencies) respectively as diode capacitance was increased. Additionally, before adding the diodes, there was a phase shift of 360° at 26.08 GHz and at 26.68 GHz when diodes were added for all capacitance values. The same phase shift was also observed at 22.7 GHz for when capacitance was 0.05pF.

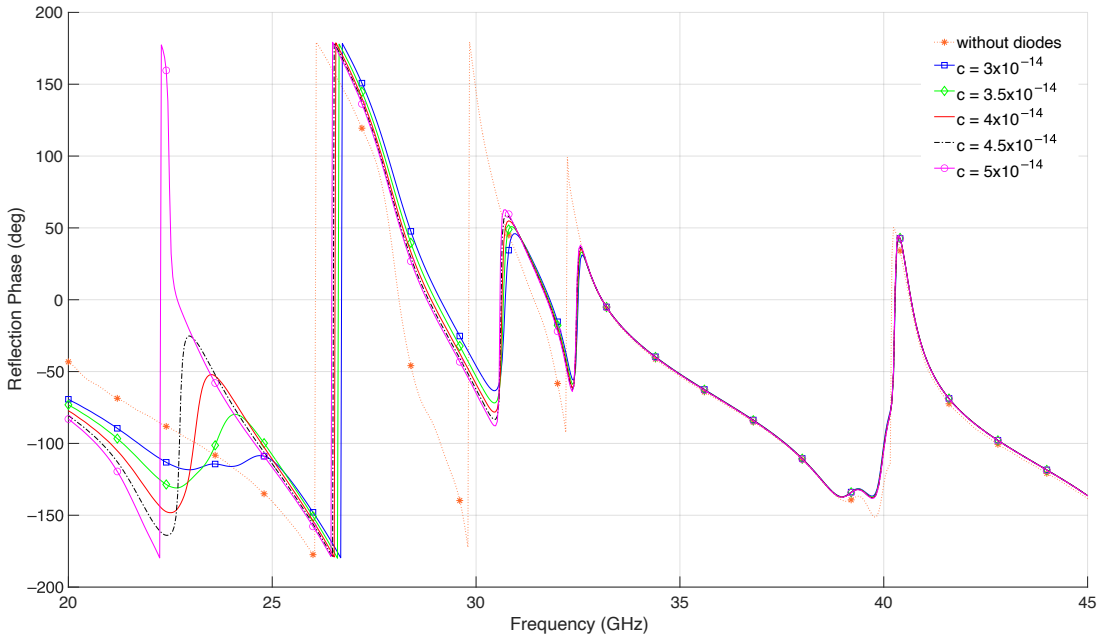

FIGURE 4.5: Reflection phase of 16 element metasurface array with and without PIN diodes.

Figure 4.5 further shows that for a frequency reconfigurable metasurface, capacitance increases when operating frequency decreases and this can be observed from equation (3.1) [182, 183].

4.4.3 Gain and Directivity

According to [177], directivity is a property of RF systems which determines how concentrated the radiation emitted is in one direction. It is a factor affecting gain in these systems. The gain describes how well the proposed structure converts input power into radio waves which travel in a particular direction [177]. Despite the fact that the gain of the metasurface antenna is closely related to its directivity, it is also a measure of its efficiency and directional capabilities [177]. The simulated results in Figure 4.6 depict the directivity and gain results before and after lumped elements were installed on the 16 element metasurface antenna. Table 4.4 shows a numerical summary of the figure.

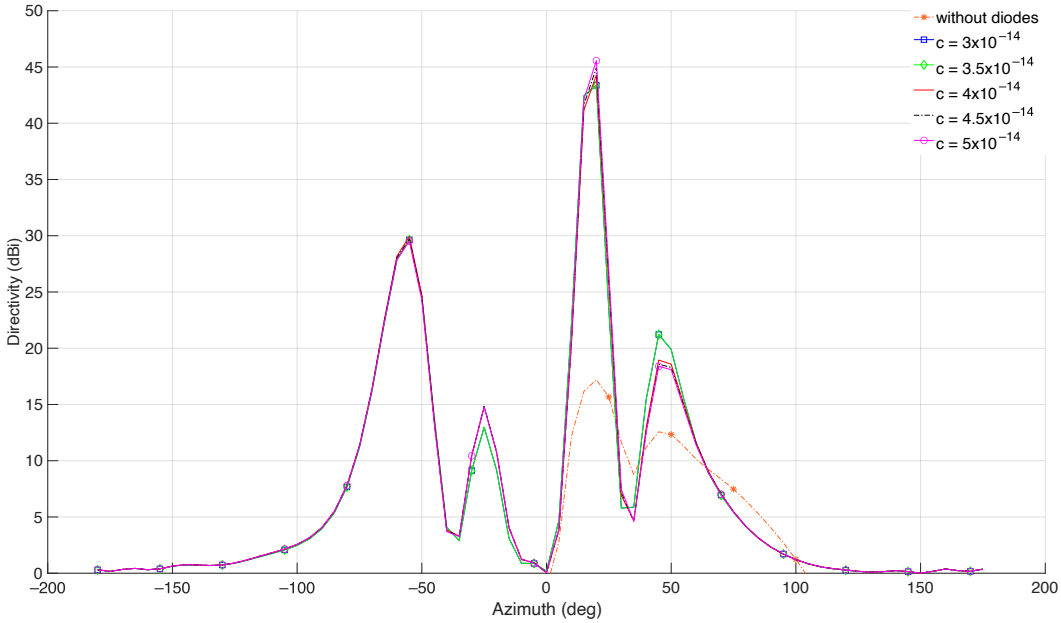

(A) Directivity

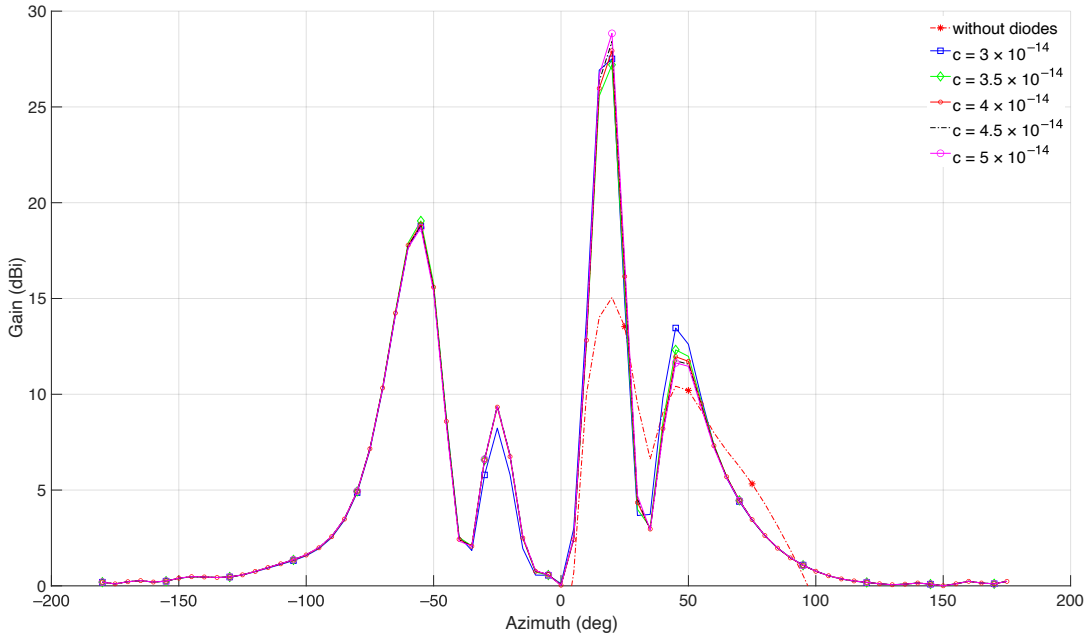

(B) Gain

FIGURE 4.6: Directivity and Gain of 16 element metasurface array with and without PIN diodes.

From Table 4.4, the gain and directivity of the reconfigurable 16 elements metasurface antenna increased from 27.23 dBi to 28.8 dBi when diodes were added. This

is due to decreased angular beamwidth which led to a narrower beam, resulting in higher directivity and gain [184]. According to authors in [185, 186], higher gain compensates for the impact of higher pathloss and is a requirement for 6G cellular communication antennas at the mmWave bands. Additionally, the directivity and gain were used to compute the radiation efficiency using equation (4.13) [177, 187]

$$\text{Radiation efficiency} = \frac{\text{Gain (dBi)}}{\text{Directivity (dBi)}} \times 100\%. \tag{4.13}$$

Since PIN diodes are connected to metallic strips of the metasurface antenna array, loss can occur due to the dissipation of power which affects the radiation efficiency. It was observed from Table 4.4 that the radiation efficiency of the metasurface antenna array decreased when diodes were added.

TABLE 4.4: Summary of gain, directivity and radiation efficiency

Capacitance (pF)	Angular Beamwidth (°)	Gain (dBi)	Directivity (dBi)	Radiation Efficiency (%)
Without diodes	16.5	15	17.2	87.2
0.03	15.3	27.23	43.37	62.79
0.035	15.0	27.50	43.06	63.86
0.04	14.5	27.93	44.28	63.08
0.045	14.31	28.42	44.93	63.25
0.05	13.9	28.8	45.6	63.31

According to [188], resistance of the diode does not affect the operating frequency. As a result, capacitance and inductance of the switches have no effect on the gain nor directivity. From Table 4.4, the directivity, gain and radiation efficiency with varying capacitances was relatively the same.

4.4.4 Effective Permittivity and Permeability

From Figure 4.7, the 16 elements metasurface antenna permittivity and permeability before and after adding diodes were all negative. These results were obtained from the CST MWS software which used a method by [189] to retrieve the effective constitutive parameters (permittivity and permeability) of a slab of metamaterial from the measurement of scattering parameters. Frequency reconfigurability can also be observed from this figure. Since μ and ϵ were negative at all resonating frequencies as shown in Figure 4.7a and 4.7b, this indicates that both the designed 4×4 metasurface antenna structure and its frequency reconfigurable structure were double negative metasurfaces which exhibits the phenomenal ability of negative refraction. Furthermore, equations (4.8) and (4.9) can be used to verify whether μ and ϵ are negative.

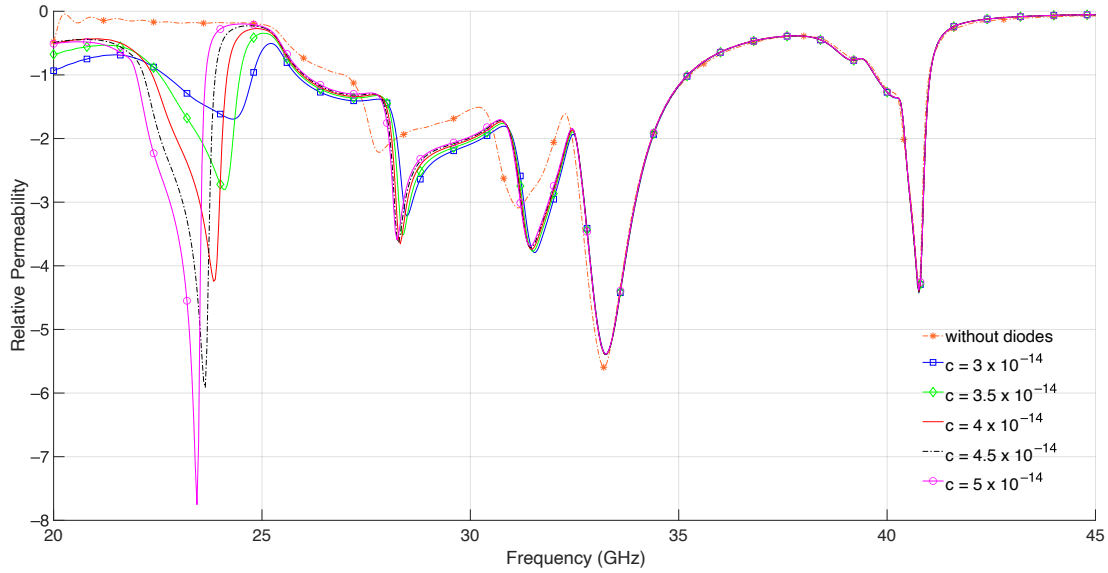

(A) effective permeability

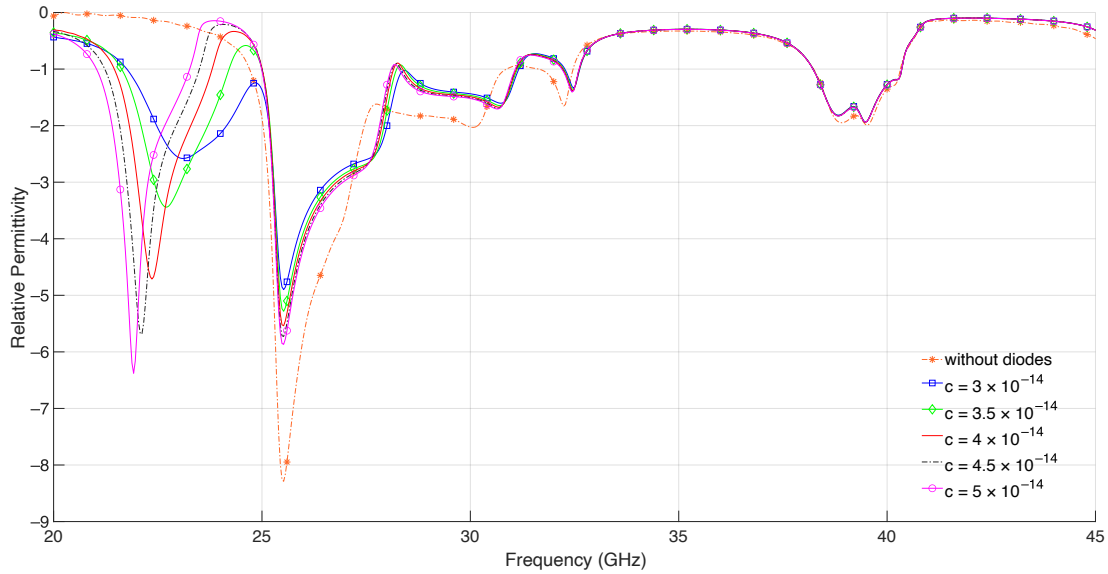

(B) effective permittivity

FIGURE 4.7: Retrieved effective constitutive parameters of the simulated results

4.4.5 Comparison with Previous Work

The performance comparisons between the proposed 16 elements frequency RMS antenna and other designs are given in Table 4.5.

TABLE 4.5: Comparisons between proposed 16 elements frequency RMS and existing designs

Ref	Size (mm^2)	Reconfiguration	Actuators	Frequency band	Detailed design procedure
[190]	2×4	Frequency	GaAs air-bridged Schottky diode	mmWave	Not specified
[129]	80×80	Pattern	12 PIN diodes	Sub-mmWave	Not specified
[170]	180×180	Frequency	Liquid metal	Sub-mmWave	Not specified
[171]	117×117	Frequency and Pattern	16 PIN diodes	mmWave	Not specified
This work	17.6×17.6	Frequency	16 PIN diodes	mmWave	Specified

It can be observed from this table that previous work did not specify how the dimensions of the metasurface were calculated.

4.5 Conclusion

In this chapter, a simple unified demonstration on how a metasurface antenna unit cell was designed theoretically from split ring resonators in order to attain its geometrical dimensions at any frequency of resonance was shown. Furthermore, a 4×4 metasurface array and frequency reconfigurable metasurface antenna with the ability to adjust its operating frequency by utilizing semiconductor diodes such as PIN diodes were proposed. The radiation mechanisms of the 16 element metasurface and RMS antenna were explained in detail via reflection phase and its magnitude characteristics. The proposed frequency RMS antenna exhibited a wideband

operational bandwidth from 25 to 32 GHz and approximately at 40 GHz. In addition, multiple gain variations from 27.33 to 28.8 dBi were observed across the full operating band at different diode capacitances. It was also observed that the gain and directivity increased when diodes were added due to decreased angular beamwidth. However, radiation efficiency decreased because of loss occurred due to the dissipation of power from the added diodes. From the proposed frequency RMS antenna, gain, directivity and radiation efficiency did not vary as frequency of operation changed. The proposed 16 elements structure has proven to be a double negative metasurface which means it has the ability to dynamically shape electromagnetic fields. Compared to previous works, the proposed work has shown a detailed design procedure.

Chapter 5

Conclusion

This thesis explores the design and implementation of frequency reconfigurable metasurface antennas which could be used in the next generation of mobile communications. An overview of RMS antenna technology which includes the main theoretical aspects and its applications in future wireless communication systems was presented. The concept of metamaterials and their 2D counterparts which are metasurfaces have been introduced, along with some of its properties and some design parameters to consider when designing RMS antennas. According to literature, split ring resonators are used to design metasurfaces. Additionally, an evaluation of metasurface antenna arrays before and after adding diodes was made.
The main findings are as follows:

- In Chapter 3, based on the analysis of the existing design process for split ring resonators, it was observed that the procedure for determining the geometrical parameters of the unit cell at any intended frequency had not been clarified. Authors in [153] presented a design procedure for a metamaterial based on SRRs. However, design parameters for the internal and external side lengths were not presented.

- Chapter 4 proposed a unified methodology for an SRR unit cell which was used to construct a 16 element metasurface antenna. The presented method

was used in the design of a PIN diode based frequency reconfigurable metasurface antenna. It was concluded that parameters such as gain and directivity of the metasurface antenna array increased with addition of diodes for frequency reconfigurability and radiation efficiency decreased. For both reconfigurable and non reconfigurable metasurface antenna array, permittivity and permeability were negative which enabled the phenomenal ability of negative refraction.

5.1 Future Work

There has been considerable success with reconfigurable metasurface antennas in the microwave regime, but the use of metasurfaces in future communication has enormous potential for further research. Metasurfaces with a stable phase and frequency response over a wide range of frequencies are key requirements for most RF applications, so future challenges will include designing them with a wide bandwidth. Additionally significant research regarding the electromagnetic properties (reflection efficiency, beamwidth, steering range and accuracy, etc.) of reconfigurable metasurface antennas needs to be largely investigated. Another important aspect would be the use of switchable or active metasurface antennas that are relatively simple to manufacture and relatively cost-effective. Metasurface antennas can introduce non-linearities when switching components are added, which would merit theoretical investigation.

Some challenging research still remains to be conducted, such as bias networks or complex designs due to scattering and/or degraded performance of reconfigurable metasurface antennas. The manufacturing of reconfigurable metasurface antennas at mmWave bands requires a decrease in unit cell dimensions. Thus, the PIN diode size becomes a significant part of the front RMS antenna area causing more absorption and diffusion. Design and implementation of off-the-shelf active components should consider size of RMS antenna unit cells in future.

References

[1] Y. Liu, X. Liu, X. Mu, T. Hou, J. Xu, M. D. Renzo, and N. Al-Dhahir, "Reconfigurable intelligent surfaces: Principles and opportunities," *IEEE Communications Surveys & Tutorials*, vol. 23, pp. 1546–1577, 2021.

[2] O. Tsilipakos, A. Tasolamprou, A. Pitilakis, F. Liu, X. chen Wang, M. Mirmoosa, D. Tzarouchis, S. Abadal, H. Taghvaee, C. Liaskos, A. Tsioliaridou, J. Georgiou, A. Cabellos-Aparicio, E. Alarcón, S. Ioannidis, A. Pitsillides, I. Akyildiz, N. Kantartzis, E. N. Economou, C. Soukoulis, M. Kafesaki, and S. Tretyakov, "Toward intelligent metasurfaces: the progress from globally tunable metasurfaces to software-defined metasurfaces with an embedded network of controllers," *Advanced Optical Materials*, vol. 8, p. 2000783, 2020.

[3] R. Alghamdi, R. Alhadrami, D. Alhothali, H. Almorad, A. Faisal, S. Helal, R. Shalabi, R. Asfour, N. Hammad, A. Shams, N. Saeed, H. Dahrouj, T. Al-Naffouri, and M.-S. Alouini, "Intelligent surfaces for 6g wireless networks: A survey of optimization and performance analysis techniques," *IEEE Access*, vol. 8, pp. 202 795–202 818, 2020.

[4] P. Yang, Y. Xiao, M. Xiao, and S. Li, "6G Wireless Communications: Vision and Potential Techniques," *IEEE Netw.*, vol. 33, no. 4, pp. 70–75, 2019.

[5] D. Kitayama, Y. Hama, K. Goto, K. Miyachi, T. Motegi, and O. Kagaya, "Transparent dynamic metasurface for a visually unaffected reconfigurable intelligent surface: controlling transmission/reflection and making a window into an rf lens," *Opt. Express*, vol. 29, no. 18, pp. 29 292–29 307, Aug 2021. [Online]. Available: http://www.osapublishing.org/oe/abstract.cfm?URI=oe-29-18-29292

[6] D. KITAYAMA, K. TATEISHI, D. KURITA, A. HARADA, M. INOMATA, T. IMAI, Y. KISHIYAMA, H. MURAI, S. ITOH, A. SIMONSSON, and P. ÖKVIST, "High speed mobility experiments on distributed mimo beamforming for 5g radio access in 28-ghz band," *IEICE Transactions on Communications*, vol. E102.B, no. 8, pp. 1418–1426, 2019.

[7] D. KURITA, K. TATEISHI, D. KITAYAMA, A. HARADA, Y. KISHIYAMA, H. MURAI, S. ITOH, A. SIMONSSON, and P. ÖKVIST, "Indoor and field experiments on 5g radio

access for 28-ghz band using distributed mimo and beamforming," *IEICE Transactions on Communications*, vol. E102.B, no. 8, pp. 1427–1436, 2019.

[8] B. A. F. Esmail, H. A. Majid, S. H. Dahlan, Z. Z. abidin, M. Himdi, R. Dewan, M. K. A. Rahim, and A. Y. I. Ashyap, "Reconfigurable metamaterial structure for 5g beam tilting antenna applications," *Waves in Random and Complex Media*, vol. 0, no. 0, pp. 1–14, 2020. [Online]. Available: https://doi.org/10.1080/17455030.2020.1720933

[9] J. Navarro-Ortiz, P. Romero-Diaz, S. Sendra, P. Ameigeiras, J. J. Ramos-Munoz, and J. M. Lopez-Soler, "A survey on 5g usage scenarios and traffic models," *IEEE Communications Surveys Tutorials*, vol. 22, no. 2, pp. 905–929, 2020.

[10] E. Basar, "Reconfigurable intelligent surface-based index modulation: A new beyond mimo paradigm for 6g," *IEEE Transactions on Communications*, vol. 68, no. 5, pp. 3187–3196, 2020.

[11] J. Zhao and Y. Liu, "A survey of intelligent reflecting surfaces (irss): Towards 6g wireless communication networks," *arXiv preprint arXiv:1907.04789*, 2019.

[12] M. Z. Chowdhury, M. Shahjalal, S. Ahmed, and Y. M. Jang, "6g wireless communication systems: Applications, requirements, technologies, challenges, and research directions," *IEEE Open Journal of the Communications Society*, vol. 1, pp. 957–975, 2020.

[13] W. Saad, M. Bennis, and M. Chen, "A Vision of 6G Wireless Systems : Applications , Trends , Technologies , and Open Research Problems 6G : Driving Trends 6G : Enabling Technologies," *IEEE Netw.*, vol. 34, no. 3, pp. 134–142, 2020.

[14] N. DOCOMO, "5g evolution and 6g, whitepaper," 2020.

[15] M. Matinmikko-Blue, S. Aalto, M. I. Asghar, H. Berndt, Y. Chen, S. Dixit, R. Jurva, P. Karppinen, M. Kekkonen, M. Kinnula, P. Kostakos, J. Lindberg, E. Mutafungwa, K. Ojutkangas, E. Rossi, S. Yrjölä, A. Öörni, P. Ahokangas, M. Z. Asghar, F. Chen, N. Iivari, M. Katz, A. Kinnula, J. Noll, H. Oinas-Kukkonen, I. Oppermann, E. Peltonen, H. Saarela, H. Saarnisaari, A. Suorsa, G. Wikstrom, and V. Ziegler, "White paper on 6g drivers and the un sdgs," *ArXiv*, vol. abs/2004.14695, 2020.

[16] E. Basar, M. Di Renzo, J. De Rosny, M. Debbah, M.-S. Alouini, and R. Zhang, "Wireless Communications Through Reconfigurable Intelligent Surfaces," *IEEE Access*, vol. 7, no. June, pp. 116 753–116 773, 2019.

[17] Q. Wu and R. Zhang, "Towards smart and reconfigurable environment: Intelligent reflecting surface aided wireless network," *IEEE Communications Magazine*, vol. 58, no. 1, pp. 106–112, 2020.

[18] Q. Wu and R. Zhang, "Intelligent reflecting surface enhanced wireless network via joint active and passive beamforming," *IEEE Transactions on Wireless Communications*, vol. 18, no. 11, pp. 5394–5409, 2019.

[19] E. Basar, "Reconfigurable Intelligent Surface-Based Index Modulation: A New Beyond MIMO Paradigm for 6G," *IEEE Trans. Commun.*, vol. 68, no. 5, pp. 3187–3196, 2020.

[20] C. Huang, A. Zappone, G. C. Alexandropoulos, M. Debbah, and C. Yuen, "Reconfigurable Intelligent Surfaces for Energy Efficiency in Wireless Communication," *IEEE Trans. Wirel. Commun.*, vol. 18, no. 8, pp. 4157–4170, 2019.

[21] S. Hu, F. Rusek, and O. Edfors, "Beyond Massive MIMO: The Potential of Data Transmission with Large Intelligent Surfaces," *IEEE Trans. Signal Process.*, vol. 66, no. 10, pp. 2746–2758, 2018.

[22] M. Cui, G. Zhang, and R. Zhang, "Secure wireless communication via intelligent reflecting surface," *IEEE Wirel. Commun. Lett.*, vol. 8, no. 5, pp. 1410–1414, 2019.

[23] X. Yu, D. Xu, and R. Schober, "Enabling secure wireless communication via intelligent reflecting surfaces," *IEEE Glob. Commun. Conf.*, pp. 1–6, 2020.

[24] Q. Wu and R. Zhang, "Intelligent Reflecting Surface Enhanced Wireless Network via Joint Active and Passive Beamforming," in *IEEE Trans. Wirel. Commun.*, vol. 18, 2019, pp. 5394–5409.

[25] H. T. Chen, A. J. Taylor, and N. Yu, "A review of metasurfaces: Physics and applications," *Reports Prog. Phys.*, vol. 79, no. 7, p. 76401, 2016. [Online]. Available: http://dx.doi.org/10.1088/0034-4885/79/7/076401

[26] S. S. Bukhari, J. Vardaxoglou, and W. Whittow, "A Metasurfaces Review: Definitions and Applications," *Appl. Sci.*, vol. 9, no. 13, p. 2727, 2019.

[27] P. Choudhury and M. A. El-Nasr, "Waves in resonant metasurfaces," *Journal of Electromagnetic Waves and Applications*, vol. 34, no. 10, pp. 1309–1313, 2020. [Online]. Available: https://doi.org/10.1080/09205071.2020.1790141

[28] N. Zheludev and Y. Kivshar, "From metamaterials to metadevices." *Nature materials*, vol. 11 11, pp. 917–24, 2012.

[29] V. G. Veselago, "Electrodynamics of substances with simultaneously negative and," *Usp. Fiz. Nauk*, vol. 92, p. 517, 1967.

[30] W. J. Krzysztofik and T. N. Cao, "Metamaterials in application to improve antenna parameters," 2018.

[31] S. Antipov, W. Liu, J. Power, and L. Spentzouris, "Left-handed metamaterials studies and their application to accelerator physics," in *Proceedings of the 2005 Particle Accelerator Conference*, 2005, pp. 458–460.

[32] X. C. Tong, *Functional metamaterials and metadevices*. Springer, 2018.

[33] R. Shelby, D. Smith, S. Nemat-Nasser, and S. Schultz, "Microwave transmission through a two-dimensional, isotropic, left-handed metamaterial," *Applied Physics Letters*, vol. 78, pp. 489–489, 2001.

[34] F. Capolino, *Theory and phenomena of metamaterials*. CRC press, 2017.

[35] C. L. Holloway, E. F. Kuester, J. A. Gordon, J. O'Hara, J. Booth, and D. R. Smith, "An overview of the theory and applications of metasurfaces: The two-dimensional equivalents of metamaterials," *IEEE Antennas and Propagation Magazine*, vol. 54, no. 2, pp. 10–35, 2012.

[36] H. L. Zhu, S. W. Cheung, and T. I. Yuk, "Mechanically pattern reconfigurable antenna using metasurface," *IET Microwaves, Antennas & Propagation*, vol. 9, no. 12, pp. 1331–1336, 2015.

[37] N. Yu and F. Capasso, "Flat optics with designer metasurfaces." *Nature materials*, vol. 13 2, pp. 139–50, 2014.

[38] K. Achouri, M. A. Salem, and C. Caloz, "General metasurface synthesis based on susceptibility tensors," *IEEE Transactions on Antennas and Propagation*, vol. 63, pp. 2977–2991, 2015.

[39] Y. Vahabzadeh, N. Chamanara, K. Achouri, and C. Caloz, "Computational analysis of metasurfaces," *IEEE Journal on Multiscale and Multiphysics Computational Techniques*, vol. 3, pp. 37–49, 2018.

[40] G. Lavigne, K. Achouri, V. S. Asadchy, S. A. Tretyakov, and C. Caloz, "Susceptibility derivation and experimental demonstration of refracting metasurfaces without spurious diffraction," *IEEE Transactions on Antennas and Propagation*, vol. 66, no. 3, pp. 1321–1330, 2018.

[41] Z. Wang, Y. Sun, L. Han, and D. Liu, "General laws of reflection and refraction for subwavelength phase grating," *arXiv: Optics*, 2013.

[42] N. Yu, P. Genevet, M. Kats, F. Aieta, J.-P. Tetienne, F. Capasso, and Z. Gaburro, "Light propagation with phase discontinuities: Generalized laws of reflection and refraction," *Science*, vol. 334, pp. 333 – 337, 2011.

[43] Q. He, S. Sun, and L. Zhou, "Tunable/reconfigurable metasurfaces: Physics and applications," *Research*, vol. 2019, 2019.

[44] A. Pitilakis, O. Tsilipakos, F. Liu, K. M. Kossifos, A. C. Tasolamprou, D.-H. Kwon, M. S. Mirmoosa, D. Manessis, N. V. Kantartzis, C. Liaskos, M. A. Antoniades, J. Georgiou, C. M. Soukoulis, M. Kafesaki, and S. A. Tretyakov, "A multi-functional reconfigurable metasurface: Electromagnetic design accounting for fabrication aspects," *IEEE Transactions on Antennas and Propagation*, vol. 69, no. 3, pp. 1440–1454, 2021.

[45] A. Shaltout, N. Kinsey, J. Kim, R. Chandrasekar, J. Ndukaife, A. Boltasseva, and V. Shalaev, "Development of optical metasurfaces: Emerging concepts and new materials," *Proceedings of the IEEE*, vol. 104, pp. 1–18, 09 2016.

[46] S. Sun, Q. He, J. Hao, S. Xiao, and L. Zhou, "Electromagnetic metasurfaces: physics and applications," *Adv. Opt. Photon.*, vol. 11, no. 2, pp. 380–479, Jun 2019. [Online]. Available: http://aop.osa.org/abstract.cfm?URI=aop-11-2-380

[47] D. R. Smith, O. Yurduseven, L. P. Mancera, P. Bowen, and N. B. Kundtz, "Analysis of a waveguide-fed metasurface antenna," *Phys. Rev. Applied*, vol. 8, p. 054048, Nov 2017. [Online]. Available: https://link.aps.org/doi/10.1103/PhysRevApplied.8.054048

[48] B. O. Zhu, K. Chen, N. Jia, L. Sun, J. Zhao, T. Jiang, and Y. Feng, "Dynamic control of electromagnetic wave propagation with the equivalent principle inspired tunable metasurface," *Scientific Reports*, vol. 4, 2014.

[49] J. Y. Dai, J. Zhao, Q. Cheng, and T. J. Cui, "Independent control of harmonic amplitudes and phases via a time-domain digital coding metasurface," *Light, Science & Applications*, vol. 7, 2018.

[50] C. Pfeiffer and A. Grbic, "Metamaterial huygens' surfaces: Tailoring wave fronts with reflectionless sheets," *Phys. Rev. Lett.*, vol. 110, p. 197401, May 2013. [Online]. Available: https://link.aps.org/doi/10.1103/PhysRevLett.110.197401

[51] S. Maci, G. Minatti, M. Casaletti, and M. Bosiljevac, "Metasurfing: Addressing waves on impenetrable metasurfaces," *IEEE Antennas and Wireless Propagation Letters*, vol. 10, pp. 1499–1502, 2011.

[52] M. Nannetti, F. Caminita, and S. Maci, "Leaky-wave based interpretation of the radiation from holographic surfaces," in *2007 IEEE Antennas and Propagation Society International Symposium*, 2007, pp. 5813–5816.

[53] L. You, J. Xu, G. Alexandropoulos, J. Wang, W. Wang, and X. Gao, "Dynamic metasurface antennas for energy efficient massive mimo uplink communications," 06 2021.

[54] C. Liaskos, S. Nie, A. Tsioliaridou, A. Pitsillides, S. Ioannidis, and I. Akyildiz, "Realizing Wireless Communication Through Software-Defined HyperSurface Environments," *19th IEEE Int. Symp. a World Wireless, Mob. Multimed. Networks, WoWMoM 2018*, 2018.

[55] A. Li, S. Singh, and D. Sievenpiper, "Metasurfaces and their applications," *Nanophotonics*, vol. 7, no. 6, pp. 989–1011, 2018. [Online]. Available: https://doi.org/10.1515/nanoph-2017-0120

[56] J. Gu, R. Singh, X. Liu, X. Zhang, Y. Ma, S. Zhang, S. Maier, Z. Tian, A. Azad, H.-T. Chen, A. J. Taylor, J. Han, and W. Zhang, "Active control of electromagnetically induced transparency analogue in terahertz metamaterials." *Nature communications*, vol. 3, p. 1151, 2012.

[57] Q. Zhao, J. Zhou, F. Zhang, and D. Lippens, "Mie resonance-based dielectric metamaterials," *Materials Today*, vol. 12, pp. 60–69, 2009.

[58] W. Padilla, A. Taylor, C. Highstrete, M. Lee, and R. Averitt, "Dynamical electric and magnetic metamaterial response at terahertz frequencies," in *2006 Conference on Lasers and Electro-Optics and 2006 Quantum Electronics and Laser Science Conference*, 2006, pp. 1–2.

[59] I. Chatzakis, L. Luo, J. Wang, N.-H. Shen, T. Koschny, J. Zhou, and C. M. Soukoulis, "Reversible modulation and ultrafast dynamics of terahertz resonances in strongly photoexcited metamaterials," *Phys. Rev. B*, vol. 86, p. 125110, Sep 2012. [Online]. Available: https://link.aps.org/doi/10.1103/PhysRevB.86.125110

[60] N. Shen, M. Massaouti, M. Gokkavas, J.-M. Manceau, E. Ozbay, M. Kafesaki, T. Koschny, S. Tzortzakis, and C. Soukoulis, "Optically implemented broadband blueshift switch in the terahertz regime," *Physical review letters*, vol. 106, p. 037403, 01 2011.

[61] A. Geim and K. Novoselov, "The rise of graphene," *Nature materials*, vol. 6, pp. 183–91, 04 2007.

[62] A. H. Castro Neto, F. Guinea, N. M. R. Peres, K. S. Novoselov, and A. K. Geim, "The electronic properties of graphene," *Reviews of Modern Physics*, vol. 81, no. 1, p. 109–162, Jan 2009. [Online]. Available: http://dx.doi.org/10.1103/RevModPhys.81.109

[63] P. A. George, J. Strait, J. Dawlaty, S. Shivaraman, M. Chandrashekhar, F. Rana, and M. G. Spencer, "Ultrafast optical-pump terahertz-probe spectroscopy of the carrier relaxation and recombination dynamics in epitaxial graphene," *Nano Letters*, vol. 8, no. 12, pp. 4248–4251, 2008, pMID: 18989983. [Online]. Available: https://doi.org/10.1021/nl8019399

[64] J. Cheng, F. Fan, and S. Chang, "Recent progress on graphene-functionalized metasurfaces for tunable phase and polarization control," *Nanomaterials*, vol. 9, 2019.

[65] S. H. Lee, M. Choi, T.-T. Kim, S. Lee, M. Liu, X. Yin, H. Choi, S. S. Lee, C.-G. Choi, S. Choi, X. Zhang, and B. Min, "Switching terahertz waves with gate-controlled active graphene metamaterials." *Nature materials*, vol. 11 11, pp. 936–41, 2012.

[66] F. Lu, B. Liu, and S. Shen, "Infrared wavefront control based on graphene metasurfaces," *Advanced Optical Materials*, vol. 2, pp. 794–799, 2014.

[67] Z.-B. Li, K. Yao, F. Xia, S. Shen, J. Tian, and Y. Liu, "Graphene plasmonic metasurfaces to steer infrared light," *Scientific Reports*, vol. 5, 2015.

[68] Y. Zhang, Y. Feng, T. Jiang, J. Cao, J. Zhao, and B. Zhu, "Tunable broadband polarization rotator in terahertz frequency based on graphene metamaterial," *Carbon*, vol. 133, pp. 170–175, 2018. [Online]. Available: https://www.sciencedirect.com/science/article/pii/S0008622318302811

[69] J. Li, P. Yu, H. Cheng, W. Liu, Z. Li, B. Xie, S. Chen, and J. Tian, "Optical polarization encoding using graphene-loaded plasmonic metasurfaces," *Advanced Optical Materials*, vol. 4, no. 1, pp. 91–98, 2016. [Online]. Available: https://onlinelibrary.wiley.com/doi/abs/10.1002/adom.201500398

[70] S. Dutta Gupta, N. Dabidian, I. Kholmanov, M. Belkin, and G. Shvets, "Electrical tuning of the polarization state of light using graphene-integrated anisotropic metasurfaces," *Philosophical Transactions of The Royal Society A Mathematical Physical and Engineering Sciences*, vol. 375, p. 20160061, 03 2017.

[71] V. V. Popov, O. Polischuk, S. Nikitov, V. Ryzhii, T. Otsuji, and M. Shur, "Amplification and lasing of terahertz radiation by plasmons in graphene with a planar distributed bragg resonator," *Journal of Optics*, vol. 15, p. 114009, 10 2013.

[72] P.-Y. Chen and J. Jung, "$\mathcal{PT}$ symmetry and singularity-enhanced sensing based on photoexcited graphene metasurfaces," *Phys. Rev. Applied*, vol. 5, p. 064018, Jun 2016. [Online]. Available: https://link.aps.org/doi/10.1103/PhysRevApplied.5.064018

[73] G. I. Kiani, K. P. Esselle, A. R. Weily, and K. L. Ford, "Active frequency selective surface using pin diodes," in *2007 IEEE Antennas and Propagation Society International Symposium*, 2007, pp. 4525–4528.

[74] D. F. Mamedes, A. Gomes Neto, J. C. e Silva, and J. Bornemann, "Design of reconfigurable frequency-selective surfaces including the pin diode threshold region," *IET Microwaves, Antennas Propagation*, vol. 12, no. 9, pp. 1483–1486, 2018.

[75] L. Subrt and P. Pechac, "Controlling Propagation Environments Using Intelligent Walls," *2012 6th Eur. Conf. Antennas Propag.*, pp. 1–5, 2012.

[76] G. H. Elzwawi, H. H. Elzuwawi, M. M. Tahseen, T. A. Denidni, and S. Member, "Frequency Selective Surface-Based Switched-Beamforming Antenna," *IEEE Access*, vol. 6, pp. 48 042–48 050, 2018.

[77] W. Li, S. Xia, B. He, J. Chen, H. Shi, A. Zhang, Z. Li, and Z. Xu, "A reconfigurable polarization converter using active metasurface and its application in horn antenna," *IEEE Transactions on Antennas and Propagation*, vol. PP, pp. 1–1, 10 2016.

[78] B. Zhu, Y. Feng, J. Zhao, C. Huang, and T. Jiang, "Switchable metamaterial reflector/absorber for different polarized electromagnetic waves," *Applied Physics Letters*, vol. 97, p. 051906, 2010.

[79] Z. Luo, J. Long, X. Chen, and D. Sievenpiper, "Electrically tunable metasurface absorber based on dissipating behavior of embedded varactors," *Applied Physics Letters*, vol. 109, p. 071107, 2016.

[80] S. V. Hum and J. Perruisseau-Carrier, "Reconfigurable reflectarrays and array lenses for dynamic antenna beam control: A review," *IEEE Trans. Antennas Propag.*, vol. 62, no. 1, pp. 183–198, 2014.

[81] E. Carrasco, M. Barba, and J. A. Encinar, "X-band reflectarray antenna with switching-beam using PIN diodes and gathered elements," *IEEE Trans. Antennas Propag.*, vol. 60, no. 12, pp. 5700–5708, 2012.

[82] J. Y. Lau and S. V. Hum, "Reconfigurable transmitarray design approaches for beamforming applications," *IEEE Transactions on Antennas and Propagation*, vol. 60, no. 12, pp. 5679–5689, 2012.

[83] C. Huang, C. Zhang, J. Yang, B. Sun, B. Zhao, and X. Luo, "Reconfigurable metasurface for multifunctional control of electromagnetic waves," *Advanced Optical Materials*, vol. 5, no. 22, p. 1700485, 2017. [Online]. Available: https://onlinelibrary.wiley.com/doi/abs/10.1002/adom.201700485

[84] H. Yang, X. Cao, F. Yang, J. Gao, S. Xu, M. Li, X. Chen, Y. Zhao, Y. Zheng, and S. Li, "A programmable metasurface with dynamic polarization, scattering and focusing control," *Sci. Rep.*, vol. 6, no. October, pp. 1–11, 2016. [Online]. Available: http://dx.doi.org/10.1038/srep35692

[85] L. Sijia, X. Cao, L. Xu, L. Zhou, H. Yang, J. Han, Z. Zhang, D. Zhang, X. Liu, C. Zhang, Y. Zheng, and Y. Zhao, "Ultra-broadband reflective metamaterial with rcs reduction based on polarization convertor, information entropy theory and genetic optimization algorithm," *Scientific Reports*, vol. 5, p. 37409, 11 2016.

[86] K. Wang, J. Zhao, Q. Cheng, D. Dong, and T. Cui, "Broadband and broad-angle low-scattering metasurface based on hybrid optimization algorithm," *Scientific reports*, vol. 4, p. 5935, 08 2014.

[87] J. Zhao, Q. Cheng, X. Wang, M. Yuan, X. Zhou, X. Fu, M. Qi, S. Liu, H. Chen, Y. Zhang, and T. Cui, "Metasurfaces: Controlling the bandwidth of terahertz low-scattering metasurfaces (advanced optical materials 11/2016)," *Advanced Optical Materials*, vol. 4, pp. 1660–1660, 11 2016.

[88] D. Kouzapas, C. Skitsas, T. Saeed, V. Soteriou, M. Lestas, A. Philippou, S. Abadal, C. Liaskos, L. Petrou, J. Georgiou, and A. Pitsillides, "Towards fault adaptive routing in metasurface controller networks," *Euromicro Newsletter*, vol. 106, Jun. 2020, funding Information: This work was partially funded by the European Union via the Horizon 2020: Future Emerging Topics call (FETOPEN), grant EU736876 , project VISORSURF (http://www.visorsurf.eu .) and Cyprus RPF HSadapt, COMPLEMENTARY/0916/0008 . Funding Information: This work was partially funded by the European Union via the Horizon 2020: Future Emerging Topics call (FETOPEN), grant EU736876, project VISORSURF (http://www.visorsurf.eu.) and Cyprus RPF HSadapt, COMPLEMENTARY/0916/0008. Publisher Copyright: © 2019.

[89] C. K. Liaskos, G. Pyrialakos, A. Pitilakis, S. Abadal, A. Tsioliaridou, A. C. Tasolamprou, O. Tsilipakos, N. V. Kantartzis, S. Ioannidis, E. Alarcón, A. Cabellos-Aparicio, M. Kafesaki, A. Pitsillides, K. M. Kossifos, J. Georgiou, and I. F. Akyildiz, "Absense: Sensing electromagnetic waves on metasurfaces via ambient compilation of full absorption," *Proceedings of the Sixth Annual ACM International Conference on Nanoscale Computing and Communication*, 2019.

[90] C.-W. Lee, H. Choi, and H. Jeong, "Tunable metasurfaces for visible and swir applications," *Nano Convergence*, vol. 7, p. 3, 12 2020.

[91] F. Ding, Y. Yang, and S. I. Bozhevolnyi, "Dynamic metasurfaces using phase-change chalcogenides," *Advanced Optical Materials*, vol. 7, no. 14, p. 1801709, 2019. [Online]. Available: https://onlinelibrary.wiley.com/doi/abs/10.1002/adom.201801709

[92] M. S. Nisar, X. Yang, L. Lu, J. Chen, and L. Zhou, "On-chip integrated photonic devices based on phase change materials," *Photonics*, vol. 8, no. 6, 2021. [Online]. Available: https://www.mdpi.com/2304-6732/8/6/205

[93] K. J. Miller, R. F. Haglund, and S. M. Weiss, "Optical phase change materials in integrated silicon photonic devices: review," *Opt. Mater. Express*, vol. 8, no. 8, pp. 2415–2429, Aug 2018. [Online]. Available: http://www.osapublishing.org/ome/abstract.cfm?URI=ome-8-8-2415

[94] T. Siegrist, P. Merkelbach, and M. Wuttig, "Phase change materials: Challenges on the path to a universal storage device," *Annual Review of Condensed Matter Physics*, vol. 3, pp. 215–237, 2012.

[95] J. Kalikka, J. Akola, and R. Jones, "Simulation of crystallization in ge2sb2te5: A memory effect in the canonical phase-change material," *Physical review. B, Condensed matter*, vol. 90, p. 184109, 11 2014.

[96] J. Skelton, A. Pallipurath, T. Lee, and S. Elliott, "Atomistic origin of the enhanced crystallization speed and n-type conductivity in bi-doped ge-sb-te phase-change materials," *Advanced Functional Materials*, vol. 24, no. 46, p. 7291, Dec. 2014.

[97] D. Lencer, M. Salinga, B. Grabowski, T. Hickel, J. Neugebauer, and M. Wuttig, "A map for phase-change materials," *Nature materials*, vol. 7, pp. 972–7, 01 2009.

[98] W. Jiang, "Nonvolatile and ultra-low-loss reconfigurable mode (de)multiplexer/switch using triple-waveguide coupler with ge2sb2se4te1 phase change material," *Scientific Reports*, vol. 8, 2018.

[99] Y. Zhang, J. Chou, J. Li, H. Li, Q. Du, A. Yadav, S. Zhou, M. Shalaginov, Z. Fang, H. Zhong, C. Roberts, P. Robinson, B. Bohlin, C. Rios Ocampo, H. Lin, M. Kang, T. Gu, J. Warner, V. Liberman, and J. Hu, "Broadband transparent optical phase change materials for high-performance nonvolatile photonics," *Nature Communications*, vol. 10, pp. 1–9, 09 2019.

[100] Z. Gong, F. Yang, L. Wang, R. Chen, J. Wu, C. P. Grigoropoulos, and J. Yao, "Phase change materials in photonic devices," *Journal of Applied Physics*, vol. 129, no. 3, p. 030902, 2021. [Online]. Available: https://doi.org/10.1063/5.0027868

[101] E. Prokhorov, J. J. Gervacio-Arciniega, G. Luna-Bárcenas, Y. Kovalenko, F. J. Espinoza-Beltrán, and G. Trápaga, "Dielectric properties of ge2sb2te5 phase-change films," *Journal of Applied Physics*, vol. 113, no. 11, p. 113705, 2013. [Online]. Available: https://doi.org/10.1063/1.4795592

[102] X. Wang, H. Qi, X. Hu, Z. Yu, S. Ding, Z. Du, and Q. Gong, "Advances in photonic devices based on optical phase-change materials," *Molecules*, vol. 26, no. 9, 2021. [Online]. Available: https://www.mdpi.com/1420-3049/26/9/2813

[103] K. E. Goodson, "Ordering up the minimum thermal conductivity of solids," *Science*, vol. 315, no. 5810, pp. 342–343, 2007. [Online]. Available: https://www.science.org/doi/abs/10.1126/science.1138067

[104] J. Cao, W. Fan, K. Chen, N. Tamura, M. Kunz, V. Eyert, and J. Wu, "Constant threshold resistivity in the metal-insulator transition of vo 2," *Physical Review B*, vol. 82, p. 241101, 2010.

[105] J. Nag, J. Ryckman, M. Hertkorn, B. Choi, R. Haglund, and S. Weiss, "Ultrafast compact silicon-based ring resonator modulators using metal-insulator switching of vanadium dioxide," *Physics and Simulation of Optoelectronic Devices XVIII*, vol. 7597, p. 759710, 03 2010.

[106] J. Ryckman, V. Diez-Blanco, J. Nag, R. Marvel, B. Choi, R. Haglund, and S. Weiss, "Photothermal optical modulation of ultra-compact hybrid si-$vo_2 ringresonators,''$ *Optics express*, $vol.$ 20, $pp.13\,215 - -25, 062012.$

[107] K. Bi, K. Huang, L. Zeng, M. Zhou, Q. Wang, G. Wang, and M. Lei, "Tunable dielectric properties of ferrite-dielectric based metamaterial," *PloS one*, vol. 10, p. e0127331, 05 2015.

[108] W. Qingmin, L. Zeng, M. Lei, and K. Bi, "Tunable metamaterial bandstop filter based on ferromagnetic resonance," *AIP Advances*, vol. 5, p. 077145, 07 2015.

[109] H. Yang, T. Yu, W. Qingmin, and M. Lei, "Wave manipulation with magnetically tunable metasurfaces," *Scientific Reports*, vol. 7, 12 2017.

[110] Y. (, Y. Huang, G. Wen, Z. (, S. (, and O. Gordon, "Tunable broadband metamaterial absorber consisting of ferrite slabs and a copper wire," *Chinese Physics B*, vol. 21, p. 038501, 03 2012.

[111] J. Gao, C. Lan, Q. Zhao, B. Li, and J. Zhou, "Electrically controlled mie-resonance absorber," *Opt. Express*, vol. 25, no. 19, pp. 22 658–22 666, Sep 2017. [Online]. Available: http://www.osapublishing.org/oe/abstract.cfm?URI=oe-25-19-22658

[112] N. Shlezinger, G. Alexandropoulos, M. Imani, Y. Eldar, and D. Smith, "Dynamic metasurface antennas for 6g extreme massive mimo communications," 06 2020.

[113] E. Basar, "Transmission through large intelligent surfaces: A new frontier in wireless communications," in *2019 European Conference on Networks and Communications (EuCNC)*, 2019, pp. 112–117.

[114] L. Lv, Q. Wu, Z. Li, N. Al-Dhahir, and J. Chen, "Secure two-way communications via intelligent reflecting surfaces," *IEEE Communications Letters*, 11 2020.

[115] K. Feng, X. Li, Y. Han, S. Jin, and Y. Chen, "Physical layer security enhancement exploiting intelligent reflecting surface," *IEEE Communications Letters*, vol. 25, pp. 734–738, 2021.

[116] N. Shlezinger, O. Dicker, Y. C. Eldar, I. Yoo, M. F. Imani, and D. R. Smith, "Dynamic metasurface antennas for uplink massive mimo systems," *IEEE Transactions on Communications*, vol. 67, pp. 6829–6843, 2019.

[117] J. Hodge and A. I. Zaghloul, "Utilizing a reconfigurable metasurface antenna as a device for spatial multiplexing and modulation," in *URSI Radio Science Meeting*, 2018.

[118] K. V. Mishra, J. A. Hodge, and A. I. Zaghloul, "Reconfigurable metasurfaces for radar and communications systems," in *2019 URSI Asia-Pacific Radio Science Conference (AP-RASC)*, 2019, pp. 1–4.

[119] T. Sleasman, M. Boyarsky, L. Pulido-Mancera, T. Fromenteze, M. F. Imani, M. S. Reynolds, and D. R. Smith, "Experimental synthetic aperture radar with dynamic metasurfaces," *IEEE Transactions on Antennas and Propagation*, vol. 65, no. 12, pp. 6864–6877, 2017.

[120] A. V. Diebold, M. F. Imani, T. Sleasman, and D. R. Smith, "Phaseless computational ghost imaging at microwave frequencies using a dynamic metasurface aperture," *Appl. Opt.*, vol. 57, no. 9, pp. 2142–2149, Mar 2018. [Online]. Available: http://www.osapublishing.org/ao/abstract.cfm?URI=ao-57-9-2142

[121] M. Boyarsky, T. Sleasman, M. Imani, J. Gollub, and D. Smith, "Electronically steered metasurface antenna," *Scientific Reports*, vol. 11, p. 4693, 02 2021.

[122] D. Rotshild and A. Abramovich, "Ultra-wideband reconfigurable x-band and ku-band metasurface beam-steerable reflector for satellite communications," *Electronics*, vol. 10, no. 17, 2021. [Online]. Available: https://www.mdpi.com/2079-9292/10/17/2165

[123] M. Boyarsky, T. Sleasman, L. Pulido-Mancera, T. Fromenteze, A. Pedross-Engel, C. M. Watts, M. F. Imani, M. S. Reynolds, and D. R. Smith, "Synthetic aperture radar with dynamic metasurface antennas: a conceptual development," *J. Opt. Soc. Am. A*, vol. 34, no. 5, pp. A22–A36, May 2017. [Online]. Available: http://www.osapublishing.org/josaa/abstract.cfm?URI=josaa-34-5-A22

[124] T. Fromenteze, M. Boyarsky, J. Gollub, T. Sleasman, M. Imani, and D. R. Smith, "Single-frequency near-field mimo imaging," in *2017 11th European Conference on Antennas and Propagation (EUCAP)*, 2017, pp. 1415–1418.

[125] L. Pulido-Mancera, T. Fromenteze, T. Sleasman, M. Boyarsky, M. F. Imani, M. Reynolds, and D. Smith, "Application of range migration algorithms to imaging with a dynamic metasurface antenna," *J. Opt. Soc. Am. B*, vol. 33, no. 10, pp. 2082–2092, Oct 2016. [Online]. Available: http://www.osapublishing.org/josab/abstract.cfm?URI=josab-33-10-2082

[126] T. Sleasman, M. Boyarsky, M. F. Imani, J. N. Gollub, and D. R. Smith, "Design considerations for a dynamic metamaterial aperture for computational imaging at microwave frequencies," *J. Opt. Soc. Am. B*, vol. 33, no. 6, pp. 1098–1111, Jun 2016. [Online]. Available: http://www.osapublishing.org/josab/abstract.cfm?URI=josab-33-6-1098

[127] T. Sharma, A. Chehri, and P. Fortier, "Reconfigurable intelligent surfaces for 5g and beyond wireless communications: A comprehensive survey," *Energies*, vol. 14, no. 24, 2021. [Online]. Available: https://www.mdpi.com/1996-1073/14/24/8219

[128] C. Saha, J. Siddiqui, D. Guha, and Y. Antar, "Square split ring resonators: Modelling of resonant frequency and polarizability," 01 2008, pp. 1 – 3.

[129] S. Chaimool, T. Hongnara, C. Rakluea, P. Akkaraekthalin, and Y. Zhao, "Design of a pin diode-based reconfigurable metasurface antenna for beam switching applications," *International Journal of Antennas and Propagation*, vol. 2019, pp. 1–7, 01 2019.

[130] L. Smith, V. Shiran, W. Gomaa, and T. Darcie, "Characterization of a split-ring-resonator-loaded transmission line at terahertz frequencies," *Opt. Express*, vol. 29, no. 15, pp. 23 282–23 289, Jul 2021. [Online]. Available: http://www.osapublishing.org/oe/abstract.cfm?URI=oe-29-15-23282

[131] L. Su, J. Naqui, J. Mata, and F. Martín, "Recent advances in modeling metamaterial transmission lines based on pairs of split ring resonators (srrs): Coupling between the srrs forming the pair," in *2014 8th International Congress on Advanced Electromagnetic Materials in Microwaves and Optics*, 2014, pp. 382–384.

[132] M. Duran-Sindreu, A. Velez, G. Siso, P. Velez, J. Selga, J. Bonache, and F. Martin, "Recent advances in metamaterial transmission lines based on split rings," *Proceedings of the IEEE*, vol. 99, no. 10, pp. 1701–1710, 2011.

[133] A. Vallecchi, E. Shamonina, and C. J. Stevens, "Analytical model of the fundamental mode of 3d square split ring resonators," *Journal of Applied Physics*, vol. 125, no. 1, p. 014901, 2019. [Online]. Available: https://doi.org/10.1063/1.5053482

[134] C. Saha, J. Y. Siddiqui, and Y. M. M. Antar, "Square split ring resonator backed coplanar waveguide for filter applications," in *2011 XXXth URSI General Assembly and Scientific Symposium*, 2011, pp. 1–4.

[135] C. Saha and J. Siddiqui, "A comparative analyis for split ring resonators of different geometrical shapes," 12 2011, pp. 1–4.

[136] J. J. Paul, A. S. Rekh, and S. P. T., "Study and analysis of various srr patch structures for energy harvesting applications," in *2020 5th International Conference on Communication and Electronics Systems (ICCES)*, 2020, pp. 326–329.

[137] J. Naqui, M. Durán-Sindreu, and F. Martín, "Novel sensors based on the symmetry properties of split ring resonators (srrs)," *Sensors (Basel, Switzerland)*, vol. 11, pp. 7545–53, 12 2011.

[138] V. Öznazlı and V. B. Ertürk, "On the use of split-ring resonators and complementary split-ring resonators for novel printed microwave elements: Simulations, experiments and discussions," 2007.

[139] E. A. Serria and M. I. Hussein, "Implications of metamaterial on ultra-wide band microstrip antenna performance," *Crystals*, vol. 10, no. 8, 2020. [Online]. Available: https://www.mdpi.com/2073-4352/10/8/677

[140] M. V. Shamonin, E. Shamonina, V. A. Kalinin, and L. Solymar, "Properties of a metamaterial element: Analytical solutions and numerical simulations for a singly split double ring," *Journal of Applied Physics*, vol. 95, pp. 3778–3784, 2004.

[141] H. Imtiaz, T. Ejaz, T. Zaidi, and Z. Khan, "Design and analysis of dual split ring resonator," 07 2019.

[142] A. Radkovskaya, M. Shamonin, C. J. Stevens, G. Faulkner, D. J. Edwards, E. Shamonina, and L. Solymar, "Resonant frequencies of a combination of split rings: Experimental, analytical and numerical study," *Microwave and Optical Technology Letters*, vol. 46, no. 5, pp. 473–476, 2005. [Online]. Available: https://onlinelibrary.wiley.com/doi/abs/10.1002/mop.21021

[143] R. Marques and F. Medina, "Role of bianisotropy in negative permeability and left-handed metamaterials," *Phys. Rev. B*, vol. 65, 04 2002.

[144] K. B. Alici and E. Ozbay, "Radiation properties of a split ring resonator and monopole composite," *Physica Status Solidi B-basic Solid State Physics*, vol. 244, pp. 1192–1196, 2007.

[145] K. Aydin, I. Bulu, K. Guven, M. Kafesaki, C. Soukoulis, and E. Ozbay, "Investigation of magnetic resonances for different split-ring resonator parameters and designs," *NEW JOURNAL OF PHYSICS*, vol. 7, 08 2005.

[146] D. Barbarić and Z. Šipuš, "Designing metasurfaces with canonical unit cells," *Crystals*, vol. 10, no. 10, 2020. [Online]. Available: https://www.mdpi.com/2073-4352/10/10/938

[147] V. Portosi, A. M. Loconsole, and F. Prudenzano, "A split ring resonator-based metamaterial for microwave impedance matching with biological tissue," *Applied Sciences*, vol. 10, no. 19, 2020. [Online]. Available: https://www.mdpi.com/2076-3417/10/19/6740

[148] M. I. Hossain, M. R. I. Faruque, M. T. Islam, and M. H. Ullah, "A new wide-band double-negative metamaterial for c- and s-band applications," *Materials*, vol. 8, no. 1, pp. 57–71, 2015. [Online]. Available: https://www.mdpi.com/1996-1944/8/1/57

[149] C. Saha and J. Siddiqui, "Theoretical model for estimation of resonance frequency of rotational circular split-ring resonators," *Electromagnetics*, vol. 32, pp. 345–355, 07 2012.

[150] D. M. Pozar, "Microwave engineering, johnwiley & sons," *Inc., New York*, pp. 367–368, 1998.

[151] I. Bahl and P. Bhartia, *Microwave solid state circuit design*. Wiley-Interscience, 2003.

[152] F. E. Terman *et al.*, "Radio engineer's handbook," 1943.

[153] G. Xavier, A. Serres, E. Costa, A. Oliveira, L. Nobrega, and V. Souza, "Design and application of a metamaterial superstrate on a bio-inspired antenna for partial discharge detection through dielectric windows," *Sensors*, vol. 19, p. 4255, 09 2019.

[154] S. Hashemi, "Microwave devices and techniques for ultra-wideband (uwb) communication systems," Ph.D. dissertation, University of Essex, 2011.

[155] M. Masoudi, M. G. Khafagy, A. Conte, A. El-Amine, B. Françoise, C. Nadjahi, F. E. Salem, W. Labidi, A. Süral, A. Gati, D. Bodéré, E. Arıkan, F. Aklamanu, H. Louahlia-Gualous, J. Lallet, K. Pareek, L. Nuaymi, L. Meunier, P. Silva, N. T. Almeida, T. Chahed, T. Sjölund, and C. Cavdar, "Green mobile networks for 5g and beyond," *IEEE Access*, vol. 7, pp. 107 270–107 299, 2019.

[156] X. Meng, M. Nekovee, and D. Wu, "Reconfigurable liquid crystal reflectarray metasurface for thz communications," in *Antennas and Propagation Conference 2019 (APC-2019)*, 2019, pp. 1–6.

[157] D. Rotshild, E. Rahamim, and A. Abramovich, "Innovative reconfigurable metasurface 2-d beam-steerable reflector for 5g wireless communication," *Electronics*, vol. 9, no. 8, 2020. [Online]. Available: https://www.mdpi.com/2079-9292/9/8/1191

[158] H. Jeong, D. H. Le, D. Lim, R. Phon, and S. Lim, "Reconfigurable metasurfaces for frequency selective absorption," *Advanced Optical Materials*, vol. 8, p. 1902182, 04 2020.

[159] H. Kamoda, T. Iwasaki, J. Tsumochi, and T. Kuki, "60-ghz electrically reconfigurable reflectarray using p-i-n diode," *2009 IEEE MTT-S International Microwave Symposium Digest*, pp. 1177–1180, 2009.

[160] W. Tian, P. Li, and L. Yuan, "Research and analysis of mems switches in different frequency bands," *Micromachines*, vol. 9, no. 4, 2018. [Online]. Available: https://www.mdpi.com/2072-666X/9/4/185

[161] S. Foo, "Liquid-crystal-tunable metasurface antennas," *2017 11th European Conference on Antennas and Propagation (EUCAP)*, pp. 3026–3030, 2017.

[162] M. Mavridou and A. P. Feresidis, "Dynamically reconfigurable high impedance and frequency selective metasurfaces using piezoelectric actuators," *IEEE Transactions on Antennas and Propagation*, vol. 64, pp. 5190–5197, 2016.

[163] B. Majumder, K. Kandasamy, J. Mukherjee, and D. Ray, "Frequency-reconfigurable slot antenna enabled by thin anisotropic double layer metasurfaces," *IEEE Transactions on Antennas and Propagation*, vol. 64, pp. 1–1, 04 2016.

[164] S. K. Patel, K. H. Shah, and Y. P. Kosta, "Frequency-reconfigurable and high-gain metamaterial microstrip-radiating structure," *Waves in Random and Complex Media*, vol. 29, no. 3, pp. 523–539, 2019. [Online]. Available: https://doi.org/10.1080/17455030.2018.1452309

[165] W. Yang, S. Chen, W. Che, Q. Xue, and Q. Meng, "Compact high-gain metasurface antenna arrays based on higher-mode siw cavities," *IEEE Transactions on Antennas and Propagation*, vol. 66, no. 9, pp. 4918–4923, 2018.

[166] H. Ma, M. Antoniou, A. G. Stove, J. Winkel, and M. Cherniakov, "Maritime moving target localization using passive gnss-based multistatic radar," *IEEE Transactions on Geoscience and Remote Sensing*, vol. 56, no. 8, pp. 4808–4819, 2018.

[167] Z. Guanxing, Z. Liu, W. Deng, and W. Zhu, "Reconfigurable metasurfaces with mechanical actuations: towards flexible and tunable photonic devices," vol. 23, no. 1, p. 013001, dec 2020. [Online]. Available: https://doi.org/10.1088/2040-8986/abcc52

[168] W. Tang, J. Y. Dai, M. Chen, X. Li, Q. Cheng, S. Jin, K.-K. Wong, and T. J. Cui, "Programmable metasurface-based rf chain-free 8psk wireless transmitter," *Electronics Letters*, vol. 55, no. 7, pp. 417–420, 2019.

[169] F. Liu, O. Tsilipakos, A. Pitilakis, A. Tasolamprou, M. Mirmoosa, N. Kantartzis, D. Kwon, M. Kafesaki, C. Soukoulis, and S. Tretyakov, "Intelligent metasurfaces with continuously tunable local surface impedance for multiple reconfigurable functions." *arXiv: Applied Physics*, 2018.

[170] T. Qian, "Reconfigurable metasurface antenna based on the liquid metal for flexible scattering fields manipulation," *Micromachines*, vol. 12, no. 3, 2021. [Online]. Available: https://www.mdpi.com/2072-666X/12/3/243

[171] W. Li, Y. M. Wang, Y. Hei, B. Li, and X. Shi, "A compact low-profile reconfigurable metasurface antenna with polarization and pattern diversities," *IEEE Antennas and Wireless Propagation Letters*, vol. 20, no. 7, pp. 1170–1174, 2021.

[172] A. Nemati, Q. Wang, M. Hong, J. Teng *et al.*, "Tunable and reconfigurable metasurfaces and metadevices," *Opto-Electronic Advances*, vol. 1, no. 5, p. 180009, 2018.

[173] O. Yurduseven, D. R. Smith, and T. Fromenteze, "Design of a reconfigurable metasurface antenna for dynamic near-field focusing," in *2018 IEEE International Symposium on Antennas and Propagation USNC/URSI National Radio Science Meeting*, 2018, pp. 1707–1708.

[174] L. Chen, Y. Ruan, and H. Y. Cui, "Liquid metal metasurface for flexible beam-steering," *Opt. Express*, vol. 27, no. 16, pp. 23 282–23 292, Aug 2019. [Online]. Available: http://www.osapublishing.org/oe/abstract.cfm?URI=oe-27-16-23282

[175] A. Abdalrazik, A. B. Abdel-Rahman, A. Allam, M. Abo-Zahhad, K. Yoshitomi, and R. K. Pokharel, "Frequency-reconfigurable dielectric resonator antenna using metasurface," *International Journal of Microwave and Wireless Technologies*, p. 1–7, 2021.

[176] K. Chang and L.-H. Hsieh, *Microwave ring circuits and related structures*. Wiley Online Library, 2004, vol. 156.

[177] Constantine A. Balanis, *Antenna Theory: Analysis and Design*, 4th ed. Wiley, 2015.

[178] M. S. Kumar and P. I. Basarkod, "A study of the effect of dielectric composition on metamaterial performance in a multilayer environment," in *2019 International Conference on Data Science and Communication (IconDSC)*, 2019, pp. 1–5.

[179] D. R. Smith, S. Schultz, P. Marko, and C. Soukoulis, "Determination of effective permittivity and permeability of metamaterials from reflection and transmission coefficients," *Physical Review B*, vol. 65, p. 195104, 2002.

[180] P. Pujari, K. Vyas, and B. K. Sharma, "Design simulation of circular patch antenna for multiband application of x band using varactor diodes," in *Proceedings of the Conference on Advances in Communication and Control Systems (CAC2S 2013)*. Atlantis Press, 2013/04, pp. 140–144. [Online]. Available: https://www.atlantis-press.com/article/6293

[181] B. Barrowes, M. Prishvin, G. Jutras, and F. Shubitidze, "High-frequency electromagnetic induction (hfemi) sensor results from ied constituent parts," *Remote Sensing*, vol. 11, no. 20, 2019. [Online]. Available: https://www.mdpi.com/2072-4292/11/20/2355

[182] O. Sydoruk, E. Tatartschuk, E. Shamonina, and L. Solymar, "Analytical formulation for the resonant frequency of split rings," *Journal of Applied Physics*, vol. 105, pp. 014 903 – 014 903, 02 2009.

[183] A. Ashoor and S. Gupta, "Metasurface reflector with real-time independent magnitude and phase control," *arXiv: Applied Physics*, 2020.

[184] R. Poisel, *Antenna systems and electronic warfare applications*. Artech House, 2012.

[185] M. Ikram, K. Sultan, M. F. Lateef, and A. S. M. Alqadami, "A road towards 6g communicationmdash;a review of 5g antennas, arrays, and wearable devices," *Electronics*, vol. 11, no. 1, 2022. [Online]. Available: https://www.mdpi.com/2079-9292/11/1/169

[186] B. Aqlan, M. Himdi, V. Hamza, and L. Le-Coq, "A 300-ghz low-cost high-gain fully metallic fabry–perot cavity antenna for 6g terahertz wireless communications," *Scientific Reports*, vol. 11, 04 2021.

[187] I. Nassar and T. Weller, "An electrically small meandered line antenna with truncated ground plane," 02 2011, pp. 94 – 97.

[188] M. Shirazi, T. Li, and X. Gong, "Effects of pin diode switches on the performance of reconfigurable slot-ring antenna," 04 2015.

[189] X. Chen, T. Grzegorczyk, B.-I. Wu, J. Pacheco, and J. Kong, "Robust method to retrieve the constitutive effective parameters of metamaterials." *Physical review. E, Statistical, nonlinear, and soft matter physics*, vol. 70 1 Pt 2, p. 016608, 2004.

[190] E. Vassos, J. Churm, J. Powell, C. Viegas, B. Alderman, and A. Feresidis, "Air-bridged schottky diodes for dynamically tunable millimeter-wave metamaterial phase shifters," *Scientific Reports*, vol. 11, 2021.